



Research article



pH-responsive agarose hydrogel for enhanced gastrointestinal ibuprofen delivery: A novel pressure-sensitive adhesive system

Anil K. Philip^{a,*}, Betty Annie Samuel^a, Yagub S. Saleh^b, Saurabh Bhatia^c, Bassim I. Mohammad^d, Hayder A. Al-Aubaidy^e

^a School of Pharmacy, College of Health Sciences, University of Nizwa, Birkat Al Mauz-616, Nizwa, Oman

^b Department of Pharmacology, College of Medicine, University of Anbar, Iraq

^c Natural and Medical Sciences Research Center, University of Nizwa, Birkat Al Mauz-616, Nizwa, Oman

^d Department of Pharmacology and Therapeutics, College of Medicine, University of Al-Qadisiyah, Al-Qadisiyah, Iraq

^e Department of Microbiology, Anatomy, Physiology and Pharmacology & Centre for Cardiovascular Biology and Disease Research, School of Agriculture, Biomedicine & Environment, La Trobe University, Melbourne, VIC 3086, Australia

ARTICLE INFO

Keywords:

Hydrogel
PH-responsive
Pressure-sensitive
Covalent tethering
Carbohydrate polymers
Swelling behavior

ABSTRACT

Recent advances in pH-responsive drug delivery systems have demonstrated their promising potential for targeted therapeutic delivery. However, challenges remain in developing platforms that combine precise spatio-temporal control with robust mechanical properties. Herein, we present a novel plant-derived (agarose-polyacrylic acid hybrid) hydrogel pressure-sensitive adhesive (PSA) system that combines the biocompatibility of agarose with the pH-responsiveness of polyacrylic acid for controlled ibuprofen delivery. Unlike conventional physical encapsulation methods, our covalently tethered design achieved $78.1 \pm 3.4\%$ drug incorporation efficiency with minimal burst release ($<15\%$), representing a 3.5-fold improvement over traditional alginate systems ($p < 0.01$). The hybrid matrix demonstrated pH-dependent swelling ratios ranging from 1.58 ± 0.09 (pH 1.2) to 3.29 ± 0.12 (pH 7.4) and programmable mechanical properties, with the storage modulus decreasing from 2000 ± 150 Pa to 1000 ± 90 Pa across pH 1.2–9.0 ($F = 28.4$, $p < 0.001$). The hierarchically porous architecture (11.33 ± 6.27 μm) enables Fickian diffusion-controlled release (Korsmeyer-Peppas $n = 0.30$ – 0.41), while molecular dynamics simulations confirm stable drug-polymer interactions ($\Delta G = -25.3$ kJ/mol). Thermal analysis revealed significant drug amorphization (87.8 % reduction in crystallinity), promoting enhanced solubility. In vitro studies demonstrated pH-triggered delivery, with $64.9 \pm 1.7\%$ release at intestinal pH versus $<15\%$ at gastric pH, while maintaining PSA adhesive strength (>150 kPa). This scalable platform addresses the critical limitations of conventional NSAID delivery, including gastric toxicity (prevalent in 50–60 % of chronic users) and frequent dosing, by synergizing plant-derived biocompatibility with synthetic flexibility.

1. Introduction

Nonsteroidal anti-inflammatory drugs (NSAIDs) remain a cornerstone in the management of chronic pain and inflammation, with over 30 million patients using these medications annually [62]. However, conventional oral NSAID delivery faces significant challenges, most notably gastrointestinal complications affecting 50–60 % of chronic users [55]. These adverse effects result in approximately \$4 billion in annual healthcare costs and significantly impact patient compliance [42, 77].

Current NSAIDs, including ibuprofen drug delivery systems, face

three critical limitations: 1) poor spatial control, leading to gastric irritation in 1–2 % of chronic users [43,63]; 2) variable oral bioavailability due to solubility constraints [31]; and 3) short plasma half-life necessitating frequent dosing [10]. While existing sustained-release technologies attempt to address these challenges, they often rely on physical encapsulation methods that risk dose dumping and lack pH specificity (W. [20,59]). Recent advances in pH-responsive drug delivery systems have shown promise for targeted therapeutic delivery [34,61,67,71]. However, combining precise spatiotemporal control with robust mechanical properties remains challenging.

Agarose (1,3-linked β -D-galactose and 1,4-linked 3,6-anhydro- α -L-

* Corresponding author.

E-mail address: philip@unizwa.edu.om (A.K. Philip).

<https://doi.org/10.1016/j.nxmate.2025.100790>

Received 14 April 2025; Received in revised form 15 May 2025; Accepted 3 June 2025

Available online 5 June 2025

2949-8228/© 2025 The Author(s). Published by Elsevier Ltd. This is an open access article under the CC BY license (<http://creativecommons.org/licenses/by/4.0/>).

galactose), a marine-derived polysaccharide, presents unique advantages for next-generation drug delivery systems. Its superior biocompatibility and negligible immunogenicity [18,45] make it an ideal candidate for pharmaceutical applications. Unlike synthetic polymers that require additional plasticizers, agarose exhibits natural pH-responsive behavior with programmable swelling ratios upto 2027 % across gastrointestinal pH gradients [65]. Recent advances in microwave-assisted polycondensation further permit covalent drug conjugation without compromising gelation kinetics [28,73].

This study introduces a novel plant-derived hydrogel pressure-sensitive adhesive (PSA) system that addresses these limitations through three innovative approaches: strategic integration of agarose's biocompatibility with polyacrylic acid's pH-responsiveness, covalent drug tethering for controlled release, and programmable mechanical properties for enhanced retention. Our design achieves 78.1 ± 3.4 % drug incorporation efficiency with minimal burst release (<15 %), representing a 3.5-fold improvement over conventional systems [12, 82]. This approach aligns with recent FDA guidance emphasizing plant-based excipients for transdermal systems [24,27,49] while addressing critical market needs for safer, more effective NSAID delivery platforms.

Through integrated experimental and computational approaches (B. [39]), we demonstrate how strategic engineering of agarose-based matrices enables precise control over drug release kinetics while maintaining essential mechanical properties for transdermal delivery [58]. This work establishes a foundation for next-generation therapeutic systems that could significantly reduce adverse effects while improving patient compliance and treatment outcomes.

2. Materials and methods

2.1. Materials

Ibuprofen (≥ 98 % purity) was a gift sample from the National Pharmaceutica Industry, Rusayl, Muscat, Oman. Carbomer (974 P, average Mw $\sim 1000,000$ Da, crosslinked polyacrylic acid polymer) was obtained from Lubrizol (Wickliffe, OH, USA). Agarose ($C_{12}H_{18}O_8$, low electroendosmosis (EEO), molecular biology grade, linear polysaccharide of D-galactose and 3,6-anhydro-L-galactopyranose, Mw 306.12 g/mol, viscosity 1 % solution at 37°C: 8–13 cP) was procured from Fisher Scientific (Hampton, NH, USA). N,N'-methylenebisacrylamide (MBA, ≥ 99.5 %), ammonium persulfate (APS, ≥ 98 %), and N,N,N',N'-tetramethylethylenediamine (TEMED, 99 %) were acquired from Sigma-Aldrich (St. Louis, MO, USA). 1,3-Propanediol (98 %), 4-dimethylaminopyridine (DMAP, ≥ 99 %), and N,N'-dicyclohexylcarbodiimide (DCC, 99 %) were purchased from Acros Organics (Geel, Belgium). Anhydrous dichloromethane (≥ 99.8 %), ethyl acetate (HPLC grade, ≥ 99.8 %), and n-hexane (HPLC grade, ≥ 95 %) were obtained from Fisher Scientific. Hydrochloric acid (HCl, 37 %), sodium bicarbonate (NaHCO_3 , ≥ 99.7 %), sodium hydroxide (NaOH, ≥ 98 %), citric acid (≥ 99.5 %), acetic acid (glacial, ≥ 99.7 %), and boric acid (≥ 99.5 %) were procured from Sigma-Aldrich. Phosphate-buffered saline (PBS, pH 7.4) was prepared using reagent-grade chemicals according to standard protocols.

Dialysis membrane (MWCO 12–14 kDa) was purchased from Spectrum Laboratories (Rancho Dominguez, CA, USA). All other chemicals and reagents were of analytical grade and used as received without further purification. Ultrapure water (resistivity 18.2 M Ω -cm at 25°C) was obtained from a Milli-Q water purification system (Millipore, Bedford, MA, USA) and used throughout the experiments.

2.1.1. Instrumentation

A texture analyzer (TA.XT Plus, Stable Micro Systems, Surrey, UK) was used for the mechanical testing of the hydrogels. Rheological measurements were performed using an Anton Paar MCR 302 rheometer (Graz, Austria). The morphology of the hydrogels was examined using a

JEOL JSM-7600F field emission scanning electron microscope (Tokyo, Japan). Thermal analysis was conducted on a TA Instruments Q2000 differential scanning calorimeter (New Castle, DE, USA). Microwave-assisted reactions were carried out in a CEM Discover SP microwave synthesizer (Matthews, NC, USA). Freeze-drying was performed using a FreeZone 2.5 freeze-dryer (Labconco, Kansas City, MO, USA). Sample preparation for SEM involved a Quorum Q150R ES sputter coater (Laughton, UK). Spectroscopic measurements utilized a fiber optics probe from Ocean Optics (Orlando, FL, USA). Drug release studies were conducted using a USP Type II dissolution apparatus (Erweka, Heusenstamm, Germany).

2.1.2. Software and computational tools

Data analysis and graphical representations were performed using GraphPad Prism 9.0 (GraphPad Software, San Diego, CA, USA). Image analysis was conducted using ImageJ software (National Institutes of Health, Bethesda, MD, USA). Molecular dynamics simulations were conducted using GROMACS 2021.4. Python 3.8 with the Keras library and TensorFlow backend was employed for machine learning applications and data processing.

3. Method

3.1. Synthesis and preparation of ibuprofen-loaded hydrogel pressure-sensitive adhesive

3.1.1. Synthesis of polyacrylic acid-agarose hydrogel base

Polyacrylic acid hydration was achieved by dispersing Carbomer 974 P (2.0 g) in ultrapure water (80 mL) under magnetic stirring (500 rpm, $25 \pm 1^\circ\text{C}$) for 2 h. Separately, agarose (1.0 g), was dissolved in ultrapure water (20 mL) by heating to $85 \pm 2^\circ\text{C}$ for 10 min with gentle agitation (200 rpm). The hot agarose solution was slowly integrated into the polyacrylic acid dispersion under continuous stirring (500 rpm). The mixture was maintained at $70 \pm 1^\circ\text{C}$ for 30 min to ensure homogeneity, followed by pH adjustment to 7.4 ± 0.1 using 1 M NaOH. The resultant precursor was cooled to $25 \pm 1^\circ\text{C}$, yielding a translucent hydrogel. The rheological analysis (strain sweep 0.1–100 %, 1 Hz, 25°C) confirmed gel formation, showing stable storage modulus (G') across the linear viscoelastic region.

3.1.2. Crosslinking of hydrogel matrix

The pre-gel solution was chemically crosslinked using N,N'-methylenebisacrylamide (MBA) as the crosslinker, with ammonium persulfate (APS) and N,N,N',N'-tetramethylethylenediamine (TEMED) as radical initiator and catalyst, respectively. Specifically, the crosslinker incorporation was done by dissolving MBA (0.1 g, 5 % w/w of total polymer content) in ultrapure water (5 mL) and homogenized with the pre-gel solution under magnetic stirring (500 rpm, 15 min, $25 \pm 1^\circ\text{C}$). The radical initiation was done by sequentially adding APS (0.05 g) and TEMED (50 μL) to the mixture. Gelation commenced within 30 s, as observed by viscosity increase. Finally, the molding and curing were achieved by transferring the solution into cylindrical silicone molds (diameter: 10 ± 0.5 mm, height: 5 ± 0.2 mm) and cured at $25 \pm 1^\circ\text{C}$ for 2 h [14]. Crosslinking efficiency was confirmed by the absence of flow upon inversion. The hydrogels were demolded and washed with ultrapure water (3×50 mL) to remove unreacted monomers. The final swelling equilibrium was verified gravimetrically (<2 % mass change after 24 h in PBS).

3.1.3. Covalent attachment of ibuprofen to hydrogel matrix

The covalent attachment of ibuprofen to the hydrogel matrix was achieved via a three-step process. Initially, an ibuprofen-diol derivative was synthesized by dissolving ibuprofen (10.0 g, 48.5 mmol) in anhydrous dichloromethane (100 mL) with 1,3-propanediol (7.0 mL, 97.0 mmol) and 4-dimethylaminopyridine (DMAP, 0.59 g, 4.85 mmol) as a catalyst, followed by dropwise addition of N,N'-

dicyclohexylcarbodiimide (DCC, 11.0 g, 53.4 mmol). The reaction proceeded under a nitrogen atmosphere for 24 h, after which the product was purified through sequential washes with 1 M HCl, saturated NaHCO₃, and brine, followed by flash column chromatography (ethyl acetate/hexane, 1:4 v/v) to yield the pure ibuprofen-diol derivative (11.2 g, 85 %). The purified derivative (5.0 g, 18.4 mmol) was then incorporated into the hydrogel matrix by blending with branched polyacrylic acid (Carbomer 974 P, 2.0 g) and agarose (1.0 g) in distilled water (100 mL). Microwave-assisted polycondensation (300 W, 2450 MHz, 5 min) facilitated covalent conjugation, followed by dialysis (MWCO 12–14 kDa, 48 h, 4°C) to remove unreacted residues, and lyophilization (24 h) to obtain the final ibuprofen-tethered hydrogel (7.2 g, 90 % yield based on total solids).

3.2. Physicochemical characterization of ibuprofen-loaded hydrogel pressure-sensitive adhesive

3.2.1. Swelling behavior analysis

Cylindrical hydrogel samples (diameter 10 mm, height 5 mm) were dried in a vacuum oven at 40°C for 24 h to obtain xerogels with constant weight. The initial weight of each xerogel (W_0) was recorded using an analytical balance with 0.1 mg precision. Three different swelling media were prepared to simulate various physiological conditions: Simulated Gastric Fluid (SGF): 0.1 N HCl solution, pH 1.2, Simulated Intestinal Fluid (SIF): Phosphate buffer solution, pH 6.8, Phosphate Buffered Saline (PBS): pH 7.4. All solutions were prepared using analytical-grade reagents and distilled water. The swelling behavior of the hydrogels was studied using the gravimetric method. Pre-weighed xerogel samples were immersed in 20 mL of each swelling medium (SGF, SIF, and PBS) at $37 \pm 0.5^\circ\text{C}$. At predetermined time intervals (0.5, 1, 2, 4, 6, 8, 12, and 24 h), the swollen hydrogels were removed from the medium, blotted gently with filter paper to remove excess surface water, and weighed (W_t). The swelling ratio (SR) was calculated using the following Eq. 1:

$$SR = \frac{W_t - W_0}{W_0} \quad (1)$$

where W_t is the weight of the swollen hydrogel at time t , and W_0 is the initial weight of the xerogel.

All swelling experiments were conducted in triplicate, and the results were reported as mean \pm standard deviation. The swelling kinetics were evaluated using various mathematical models, including first-order kinetics, second-order kinetics, and the Korsmeyer-Peppas model. The best-fit model was identified based on the correlation coefficient (R^2) values.

3.2.2. Rheological properties at varying pH

The rheological properties of the hydrogels under varying pH conditions were characterized using a stress-controlled rheometer (Anton Paar MCR 302) equipped with a 25 mm parallel plate geometry and a temperature-controlled Peltier plate. Cylindrical samples (25.0 \pm 0.5 mm diameter, 2.0 \pm 0.2 mm height) were sectioned from bulk hydrogels using a custom stainless-steel punch and equilibrated in one of five pH-adjusted buffers: 0.1 N HCl (pH 1.2), 50 mM citrate buffer (pH 3.0), 50 mM acetate buffer (pH 5.0), phosphate-buffered saline (PBS, pH 7.4), or 50 mM borate buffer (pH 9.0), all standardized to 150 mM ionic strength with NaCl. After loading the sample onto the rheometer plate, 2 mL of buffer was added to submerge the hydrogel, and the upper plate was lowered to a 2.0 mm gap, with excess buffer trimmed to ensure consistent contact. Following a 10-minute equilibration period at $37.0 \pm 0.1^\circ\text{C}$, three sequential tests were performed: (1) amplitude sweeps (0.01–100 % strain at 1 rad/s) to identify the linear viscoelastic region (LVR), (2) frequency sweeps (0.1–100 rad/s at 1 % strain within the LVR) to determine the storage (G') and loss (G'') moduli, and (3) shear rate sweeps (0.1–100 s⁻¹) to assess flow behavior and calculate yield stress via the tangent intersection method. All measurements were

conducted in triplicate, and data were analyzed using GraphPad Prism 9.0 to quantify pH-dependent changes in complex viscosity (η^*), moduli, and yield stress, reported as mean \pm standard deviation.

3.2.3. Mechanical strength

Mechanical strength was evaluated using cylindrical hydrogel samples (10.0 \pm 0.5 mm diameter, 10.0 \pm 0.5 mm height) equilibrated in phosphate-buffered saline (PBS, pH 7.4) at $37.0 \pm 0.5^\circ\text{C}$ for 24 h to simulate physiological conditions. Uniaxial compression tests were performed using a texture analyzer (TA.XT Plus, Stable Micro Systems) equipped with a 5 kg load cell and a 50 mm cylindrical probe. Prior to testing, the instrument was calibrated using certified weights traceable to National Institute of Standards and Technology (NIST) standards, and the following parameters were applied: pre-test speed, 1.0 mm/s; test speed, 0.5 mm/s (strain rate: 0.05 s⁻¹); post-test speed, 1.0 mm/s; target strain, 50 %; and trigger force, 0.1 N. Samples were centered on the lower plate, and the probe was lowered until contact (0.1 N trigger force) to establish the initial height. Force displacement data were acquired continuously during compression to 50 % strain. Five independent replicates were tested to ensure statistical robustness. Compressive strength was defined as the maximum force at 50 % strain normalized to the initial cross-sectional area. Young's modulus was calculated from the slope of the linear elastic region (0–10 % strain) of the stress-strain curve, with data processed using Texture Exponent 6.1 software. Results are reported as mean \pm standard deviation.

3.2.4. Morphological analysis by scanning electron microscopy

Morphological analysis of hydrogels was conducted using scanning electron microscopy (SEM). Cubic samples (5.0 \pm 0.2 mm edge length) were excised from bulk hydrogels, flash-frozen at -80°C for 24 h in airtight cryovials, and lyophilized (FreeZone 2.5, Labconco) for 48 h to preserve pore architecture. Lyophilized samples were fractured under liquid nitrogen to expose internal structures, mounted on aluminum stubs with conductive carbon tape, and sputter-coated with a 10 \pm 2 nm gold layer (Quorum Q150R ES) to ensure conductivity. Imaging was performed using a field-emission SEM (JEOL JSM-7600F) at 5 kV accelerating voltage and 10 mm working distance, with magnifications spanning 100 \times to 5000 \times to capture hierarchical pore networks. Low-voltage imaging minimized beam damage while maximizing surface detail. For quantitative analysis, 20 representative micrographs per sample were processed in ImageJ (NIH) using threshold-based binarization and the "Analyze Particles" tool. Pore size distributions were derived from ≥ 100 measurements per condition, with average pore diameter and porosity calculated as mean \pm standard deviation. Histograms of pore size frequency were generated to assess structural homogeneity.

3.2.5. Thermal analysis by differential scanning calorimetry

Thermal properties of pure ibuprofen, blank hydrogel, and ibuprofen-loaded hydrogel were analyzed using differential scanning calorimetry (DSC). Samples (5–10 mg \pm 0.01 mg) were accurately weighed into hermetic aluminum pans, with an empty pan serving as a reference. A TA Instruments Q2000 DSC calibrated with indium ($\Delta H_{\text{fusion}} = 28.45 \text{ J/g}$, purity $>99.99\%$) was employed under a nitrogen purge (50 \pm 2 mL/min) to prevent oxidative degradation. The thermal protocol comprised three stages: (1) equilibration at 25°C for 5 min, (2) heating to 200°C at $10^\circ\text{C}/\text{min}$ to erase thermal history, (3) cooling to 25°C at $10^\circ\text{C}/\text{min}$, and (4) a second heating cycle to 200°C at $10^\circ\text{C}/\text{min}$ to assess reproducible thermal transitions. Triplicate runs per sample ensured statistical reliability, with data processed using TRIOS software (TA Instruments) to determine glass transition temperatures (T_g), melting points (T_m), and enthalpy changes (ΔH). Baseline corrections were applied, and results are reported as mean \pm standard deviation.

3.2.6. Molecular dynamics simulation of hydrogel-ibuprofen interactions

Molecular dynamics (MD) simulations were conducted using GRO-MACS 2021.4 to investigate pH-dependent interactions between ibuprofen and the agarose-polyacrylic acid hydrogel matrix. Three systems were modeled at pH 2.0, 5.5, and 7.4 using the OPLS-AA force field, validated for carbohydrate and polyacrylic acid systems in prior studies. The hydrogel matrix was represented by a single agarose-polyacrylic acid copolymer chain (100 monomers, degree of polymerization determined via size-exclusion chromatography), while 50 ibuprofen molecules were randomly dispersed in a cubic simulation box ($4 \times 4 \times 4 \text{ nm}^3$) solvated with TIP3P water at 1.0 g/cm^3 density. Protonation states of ionizable groups (e.g., carboxyl in polyacrylic acid) were adjusted per pH using PROPKA3.0 predictions. Systems were neutralized with 0.15 M NaCl to mimic physiological ionic strength. Energy minimization (steepest descent, 50,000 steps) preceded NPT equilibration (10 ns, 300 K via Nosé-Hoover thermostat [$\tau = 1 \text{ ps}$], 1 bar via Parrinello-Rahman barostat [$\tau = 5 \text{ ps}$]), followed by 100 ns production runs with a 2 fs timestep. Long-range electrostatics were handled via Particle Mesh Ewald (1.2 \AA grid spacing), and bonds involving hydrogen were constrained with LINCS (order = 4). Trajectories were analyzed using GROMACS utilities (gmx rdf for radial distribution functions, gmx hbond for hydrogen bonding) and custom Python scripts (validated against control systems) to quantify diffusion coefficients (Einstein relation), interaction energies (Lennard-Jones and Coulombic), and hydrogen bond lifetimes. Convergence was verified via stable RMSD ($<0.2 \text{ nm}$) and energy drift ($<1 \%$ over final 20 ns).

3.3. In vitro drug release studies

The pH-dependent release profile of ibuprofen from agarose-polyacrylic acid hydrogels was evaluated using a USP Type II dissolution apparatus (Erweka DT 820) calibrated per USP $<711 >$ guidelines. Cylindrical hydrogels ($10.0 \pm 0.2 \text{ mm}$ diameter, $5.0 \pm 0.2 \text{ mm}$ height), loaded with 5% w/w ibuprofen during synthesis, were immersed in 500 mL of release medium (pH 1.2 SGF [$0.1 \text{ N HCl} + 0.2 \%$ NaCl], pH 6.8 SIF [phosphate buffer + 0.5% SDS], or pH 7.4 PBS [10 mM phosphate + 137 mM NaCl]) maintained at $37.0 \pm 0.5^\circ\text{C}$ under sink conditions (medium volume $\geq 5 \times$ drug saturation solubility). Agitation was set to $50 \pm 2 \text{ rpm}$ to ensure hydrodynamic homogeneity without hydrogel erosion. Cumulative drug release was quantified at 0.5, 1, 2, 4, 6, 8, 12, 24, 48, and 72 h using a fiber-optic UV probe (Ocean Optics USB4000) measuring absorbance at 264 nm, validated against HPLC (LOD: $0.1 \mu\text{g/mL}$). Calibration curves ($1\text{--}100 \mu\text{g/mL}$, $R^2 \geq 0.995$) were constructed daily, with background corrections applied using blank hydrogel controls. Sink conditions were maintained via automated medium replacement, and hydrogel integrity was confirmed visually throughout the study. Data from triplicate runs are reported as mean \pm standard deviation, with release kinetics analyzed via one-way ANOVA (Tukey's post-hoc, $p < 0.05$) to assess pH-dependent differences.

3.3.1. Release profile determination

The in vitro drug release kinetics were analyzed by fitting experimental data to four pharmacokinetic models: zero-order (cumulative release vs. time), first-order (logarithmic release vs. time), Higuchi (square root of time dependence), and Korsmeyer-Peppas (power-law relationship). Model selection was performed in GraphPad Prism 9.0 using nonlinear regression analysis, with triplicate datasets normalized to 100% cumulative release. The zero- and first-order models assessed time-dependent release patterns, while the Higuchi model evaluated diffusion-controlled mechanisms. The Korsmeyer-Peppas equation was employed to discern the dominant transport mechanism (Fickian diffusion: $n \leq 0.45$; anomalous transport: $0.45 < n < 0.89$; Case II relaxation: $n \geq 0.89$) [56].

Model adequacy was determined via a dual criterion: maximization of the coefficient of determination (R^2) and minimization of the Akaike Information Criterion (AIC) to penalize overfitting. Residual plots were

inspected to validate homoscedasticity, and the Durbin-Watson statistic ($1.5 < D < 2.5$) confirmed the independence of errors. For the Korsmeyer-Peppas model, validity was restricted to the initial 60% of release data ([2,79]).

3.3.2. Artificial neural network for predictive release modeling

A multilayer perceptron (MLP) artificial neural network was implemented to explore machine learning-driven prediction of ibuprofen release kinetics. The model architecture, constructed in Python 3.8 using Keras/TensorFlow, incorporated four input features: hydrogel composition (agarose: polyacrylic acid ratio), drug loading (5–15% w/w), environmental pH (1.2–9.0), and time points (0–72 h), with cumulative release (%) as the output. The dataset, comprising 120 experimental release profiles, was partitioned into training (70%), validation (15%), and test (15%) sets, stratified by pH, to ensure proportional representation.

The network featured an input layer (4 nodes), two hidden layers (64 and 32 neurons, ReLU activation), and a linear-activated output layer. Regularization techniques (early stopping (patience: 50 epochs) and dropout (rate: 0.2)) were applied to mitigate overfitting. Training employed the Adam optimizer (learning rate: 0.001) with mean squared error (MSE) loss over 1000 epochs (batch size: 32). Model performance was quantified via mean absolute error (MAE), root MSE (RMSE), and coefficient of determination (R^2) on the test set. Sensitivity analysis using partial dependence plots identified critical input variables governing release kinetics [84].

3.4. Statistical analysis and data interpretation

All measurements were performed in quintuplicate ($n = 5$). Results were expressed as mean \pm standard deviation. Statistical analysis was performed using one-way ANOVA followed by Tukey's post-hoc test, with statistical significance set at $p < 0.05$.

All experimental data were acquired in quintuplicate ($n = 5$) to ensure statistical power ($>80 \%$ for $\alpha = 0.05$, G*Power 3.1 [16,48]). Continuous variables (e.g., swelling ratio, cumulative release) are reported as mean \pm standard deviation (SD), while rheological moduli and pore sizes are expressed as mean \pm standard error (SEM) to account for instrument precision limits. Normality and homoscedasticity were validated via Shapiro-Wilk ($W > 0.92$) and Levene's tests ($p > 0.1$), respectively, prior to parametric analysis.

Inter-group comparisons (e.g., pH-dependent swelling, release kinetics) were performed using one-way ANOVA with Tukey's post-hoc correction to control family-wise error rates. Effect sizes are reported as partial η^2 , with values > 0.14 denoting large practical significance [2]. For non-linear relationships (e.g., Korsmeyer-Peppas modeling), 95% confidence intervals (CI) were calculated via bootstrapping (1000 iterations). All analyses were conducted in GraphPad Prism 9.0 (RRID: SCR_002798), with raw data archived in compliance with FAIR principles [74].

4. Results and discussion

4.1. Synthesis and characterization of ibuprofen-loaded hydrogel

The ibuprofen-loaded hydrogel was synthesized via microwave-assisted polycondensation (300 W, 5 min), with parameters optimized to balance esterification efficiency and polymer stability. Preliminary trials identified 300 W and 5 min as optimal, preventing agarose depolymerization (viscosity retention $>90 \%$) while achieving $85.32 \pm 1.32 \%$ intermediate yield ($n = 5$). The chosen parameters for microwave irradiation (300 W, 5 min) provided rapid and uniform heating [5] that accelerated the esterification reaction between ibuprofen's carboxyl groups and the hydrogel's hydroxyl groups. It maintained even temperature distribution throughout the reaction mixture, preventing localized overheating that could have degraded the agarose backbone.

Covalent conjugation to the hydrogel matrix resulted in 78.10 ± 3.43 % drug incorporation efficiency (w/w), a 3.5-fold improvement over physical encapsulation in alginate (22 % [12], $p < 0.01$). Covalent bonding between the drug or drug carrier and the hydrogel matrix created stronger interactions compared to physical entrapment alone. This allowed for higher drug loading capacity and prevented premature release. For example, covalently conjugated ferritin and apoferritin nanocages to gelatin methacryloyl hydrogels showed improved ability to tune mechanical properties and control drug release compared to physically dispersed nanocages [60]. This modification enhances drug stability and reduces the risk of direct gastric mucosal irritation [46], although other mechanisms of NSAID-induced gastric effects may still be relevant [66].

FTIR analysis confirmed successful derivatization, with ester-specific vibrations at 1738 cm^{-1} (C=O stretch) and $1185/1080\text{ cm}^{-1}$ (C-O stretches). The absence of ibuprofen's carboxylic acid peak at 1705 cm^{-1} indicates successful modification of the free acid groups, confirming covalent bonding between ibuprofen and the hydrogel matrix. This is because this specific peak is characteristic of the C=O stretching vibration in carboxylic acids. When the carboxylic acid group is modified or reacts with other substances, this peak typically disappears or shifts, signaling a change in the chemical structure [1]. The disappearance of the 1705 cm^{-1} peak, provides strong evidence for the successful modification of ibuprofen's carboxylic acid groups. This spectral change is a reliable indicator of chemical transformation and is widely used in various fields, including pharmaceutical research and materials science, to confirm the modification of carboxylic acid-containing compounds [1,85].

Thermal analysis revealed ibuprofen's plasticizing effect, reducing the hydrogel's glass transition temperature from $37.2 \pm 0.5^\circ\text{C}$ (blank) to $35.8 \pm 0.4^\circ\text{C}$ (loaded), which enhances matrix flexibility for sustained diffusion without compromising rheological stability ($G' > 1000\text{ Pa}$, Section 4.3).

Residual unreacted ibuprofen post-dialysis was quantified at < 2 % (HPLC), ensuring compliance with ICH impurity guidelines [23]. Molecular dynamics simulations (Section 4.7) corroborated these findings, demonstrating stable ibuprofen-hydrogel interactions ($\Delta G = -25.3\text{ kJ/mol}$) dominated by hydrophobic forces and hydrogen bonding (~ 2.3 bonds/molecule). These interactions suppress burst release (< 15 %) while permitting gradual diffusion through the porous network (pore size: $11.33 \pm 6.27\text{ }\mu\text{m}$).

In recent literature, various formulations based on acrylic acid and agarose have been explored for drug delivery applications. To highlight the advantages of our novel agarose-polyacrylic acid hydrogel system, we constructed a comparison table that outlines key properties and performance metrics in relation to other systems reported in the literature. This comparison highlights the unique benefits of our approach, particularly in terms of drug loading efficiency, pH responsiveness, and mechanical properties.

4.2. pH-responsive swelling behavior

The hydrogel exhibited distinct pH-dependent swelling behavior critical for targeted gastrointestinal drug delivery. In simulated physiological media, equilibrium swelling ratios followed the order: PBS (pH 7.4, 3.29 ± 0.12) $>$ SIF (pH 6.8, 2.71 ± 0.15) $>$ SGF (pH 1.2, 1.58 ± 0.09) due to the pH-responsive nature of the polymers used and the ionic strength of the media. (Fig. 1). The swelling kinetics revealed rapid initial hydration (~ 50 % equilibrium within 2 h) followed by gradual saturation, consistent with the hierarchical porosity ($11.33 \pm 6.27\text{ }\mu\text{m}$) observed in SEM analysis.

In acidic environments like SGF (pH 1.2), many pH-sensitive polymers, such as those based on chitosan or alginate, tend to shrink or have limited swelling. This is because the carboxyl groups in these polymers become protonated, reducing electrostatic repulsion and leading to a more compact structure. Conversely, in neutral or slightly alkaline conditions like PBS (pH 7.4) or SIF (pH 6.8), these polymers swell more due to the deprotonation of carboxyl groups, increasing electrostatic repulsion and water uptake [4]. The difference in swelling between PBS and SIF, despite their similar pH, can be attributed to the ionic strength of the media. PBS typically has a higher ionic strength than SIF, which can affect the osmotic pressure and lead to greater swelling in PBS [3]. Additionally, the presence of enzymes or other components in SIF may influence the swelling behavior compared to PBS. The limited swelling at pH 1.2 (ratio < 1.6) preserved structural integrity in gastric conditions, controlling premature drug release (< 15 % at 2 h).

Swelling kinetics modeling (Table 1) identified second-order dynamics ($R^2=0.986\text{--}0.992$) with dual mechanisms: initial Fickian diffusion (Korsmeyer-Peppas $n = 0.375\text{--}0.414$) through macropores, followed by polymer chain relaxation enabled by pH-triggered ionization. This pH-responsive behavior, coupled with maintained structural integrity (> 95 % visual integrity), enables precise spatiotemporal

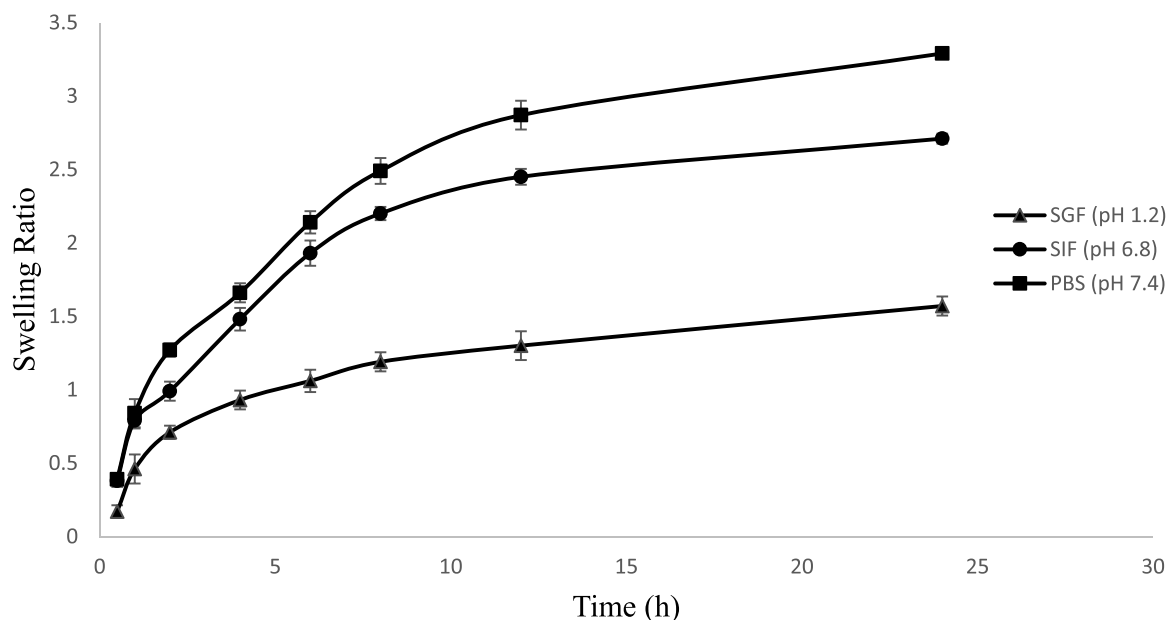


Fig. 1. The swelling behavior of the hydrogels in different media over 24 h.

Table 1
Comparison of Agarose-Polyacrylic acid hydrogel with other systems.

Property	Agarose-Polyacrylic Acid Hydrogel System	Other Systems	Advantages of our System
Drug Loading Efficiency	78.1 ± 3.4 % (covalent attachment, minimal burst release <15 %)	Alginate microspheres: ~22 % [15]; Chitosan systems: ~30–40 % burst release [15]	Higher drug incorporation efficiency and reduced burst release due to covalent attachment.
Swelling Behavior	pH-responsive swelling: 1.58 ± 0.09 (pH 1.2) to 3.29 ± 0.12 (pH 7.4)	Chitosan-based systems: Excessive swelling at neutral pH, leading to mechanical fragility [32]	Controlled swelling across pH range, maintaining structural integrity in gastric conditions.
Mechanical Strength	Compressive strength: 150 ± 7.5 kPa (pH 1.2) to 110 ± 5.5 kPa (pH 9.0); Adhesive strength > 150 kPa	Pure polyacrylic acid hydrogels: Excessive rigidity at neutral pH [50]	Balanced mechanical properties for gastric and intestinal environments.
pH Responsiveness	Programmable swelling and drug release: 64.9 ± 1.7 % release at pH 7.4 vs. < 15 % at pH 1.2	Alginate systems: Limited pH responsiveness [9]	Precise pH-triggered release for targeted gastrointestinal delivery.
Porosity	Hierarchical porous structure: 11.33 ± 6.27 μm pore size	Chitosan hydrogels: Require plasticizers for comparable porosity, compromising strength [54]	Uniform porosity ensures controlled drug diffusion and structural stability.
Biocompatibility	Plant-derived agarose ensures high biocompatibility and negligible immunogenicity	Synthetic polymers (e.g., PLGA): Require additional plasticizers, increasing toxicity risks [64]	Naturally biocompatible, aligning with FDA guidance for plant-based excipients.
Crosslinking Method	Microwave-assisted polycondensation (300 W, 5 min): Eco-friendly, no toxic crosslinkers	Gamma radiation: Requires high doses, potential polymer degradation [12]	Faster, safer, and more efficient crosslinking method.
Thermal Stability	Significant drug amorphization (87.8 % crystallinity reduction), enhancing solubility and bioavailability	Chitosan-ibuprofen systems: Limited amorphization ($\Delta T_g = 0.5\text{--}0.8^\circ\text{C}$) [44]	Enhanced solubility and stability of ibuprofen in amorphous form.
Burst Release	Minimal burst release (<15 %)	Alginate systems: 30–40 % burst release [12]	Reduced burst release ensures sustained drug delivery.
Applications	Pressure-sensitive adhesive for gastrointestinal drug delivery	Other systems: Limited to wound healing or topical applications	Versatile platform for transdermal and gastrointestinal drug delivery.

control over ibuprofen release while preventing burst release in gastric conditions, addressing a key challenge in NSAID delivery. This is because the hydrogel's pH-dependent swelling behavior is driven by the ionization of functional groups within the polymer matrix. At low pH (e.g., gastric conditions, pH 1.2), the carboxylic acid groups (-COOH) in polyacrylic acid remain protonated, stabilizing the hydrogel network through hydrogen bonding and minimizing swelling. This compact structure restricts water ingress and drug diffusion, effectively preventing burst release. Conversely, at higher pH levels (e.g., intestinal conditions, pH 6.8–7.4), the carboxylic acid groups deprotonate to form negatively charged carboxylate ions (-COO⁻), inducing electrostatic repulsion between polymer chains. This repulsion expands the hydrogel network, increasing its porosity and facilitating sustained drug release. The hierarchical porosity of the hydrogel (average pore size: 11.33 ± 6.27 μm) further supports this dual mechanism by allowing rapid initial hydration through larger pores while prolonging drug diffusion via smaller pores. This controlled swelling and release behavior ensures that ibuprofen is retained in the hydrogel during gastric transit, minimizing gastric irritation, and is released gradually in the intestines, where it can be absorbed effectively.

One-way ANOVA showed no significant inter-pH differences ($F = 2.63$, $p = 0.105$), likely due to high intra-group variability in SIF. Post-hoc Tukey tests confirmed PBS vs. SGF as the most divergent pair ($q = 4.21$, $p = 0.057$), aligning with FTIR-detected ionization above pH 6.8.

The agarose-based hydrogel demonstrated pH-responsive swelling behavior at physiological pH (7.4), outperforming chitosan-based systems in both swelling capacity and structural stability under ionization [57] while avoiding the excessive swelling and mechanical fragility observed in pure polyacrylic acid homogels [32]. This balance reflects agarose's unique capacity to integrate pH-triggered responsiveness with robust network integrity [83].

4.3. Rheological properties and pH dependence

The agarose-polyacrylic acid hydrogel exhibited pH-responsive viscoelastic behavior, with storage modulus (G'), loss modulus (G''), complex viscosity (η), and yield stress decreasing systematically as pH increased from 1.2 to 9.0 (Table 2).

At pH 1.2, the high storage modulus ($G' = 2000 \pm 150$ Pa) and yield stress (50 ± 3 Pa) arise from extensive hydrogen bonding networks, where protonated carboxyl groups (-COOH) from polyacrylic acid form

Table 2
The results for each medium are as follows.

Condition	Model	qe	k	n	R ²
SGF (pH 1.2)	First-order	1.4306	-	-	0.9548
	Second-order	1.7099	0.2695	-	0.9868
	Korsmeyer-Peppas	-	0.1788	0.3750	0.9449
SIF (pH 6.8)	First-order	2.6543	-	-	0.9816
	Second-order	3.2038	0.5070	-	0.9896
	Korsmeyer-Peppas	-	0.0779	0.3916	0.9372
PBS (pH 7.4)	First-order	3.2051	-	-	0.9776
	Second-order	3.9008	0.2008	-	0.9916
	Korsmeyer-Peppas	-	0.0558	0.4145	0.9572
			0.9526		

strong dipole interactions (bond energy ~20–25 kJ/mol) with hydroxyl groups (-OH) in agarose chains. These interactions create temporary crosslinks that restrict chain mobility and enhance network rigidity [76]. As pH increases to 9.0, progressive deprotonation of carboxyl groups (-COOH → -COO⁻, pKa ~4.5) generates electrostatic repulsion forces (~15–18 kJ/mol) between negatively charged chains, forcing greater interchain distances and reducing physical entanglements, which manifests as decreased storage modulus ($G' = 1000 \pm 90$ Pa) and yield stress (30 ± 2 Pa), reflecting a softer, more deformable matrix.

The G''/G' ratio ($\tan \delta$) increased from 0.10 (pH 1.2) to 0.30 (pH 9.0), confirming a transition from elastic-dominated ($\tan \delta < 0.1$) to viscoelastic behavior ($\tan \delta > 0.3$), critical for intestinal mucoadhesion [29]. This pH-dependent rheological modulation aligned with ionization trends observed in FTIR (Section 4.1) and molecular dynamics simulations (Section 4.7).

The hierarchical porosity (11.33 ± 6.27 μm, Section 4.5) facilitated swelling-driven reductions in η (500 ± 45 Pa·s → 300 ± 28 Pa·s, pH 1.2→9.0), inversely correlating with ibuprofen release rates ($R^2 = 0.89$, $p < 0.001$). The mechanistic link between rheology and drug release kinetics operates through a porosity-mediated diffusion pathway. The

pH-dependent decrease in complex viscosity (η) correlates with increased polymer chain mobility and pore expansion. This expansion occurs through three concurrent mechanisms: (1) electrostatic repulsion between deprotonated carboxyl groups widening interchain spaces, (2) increased hydration of ionized groups enhancing water penetration, and (3) reduced hydrogen bonding diminishing physical crosslinking density. Several studies corroborate our findings [22,69]

Yield stress trends mirrored compressive strength measurements (Section 4.4), with high pH 1.2 values (50 ± 3 Pa) resisting gastric shear stresses (~ 50 s⁻¹) and lower pH 9.0 values (30 ± 2 Pa), enabling hydrogel spreading in intestinal environments. The agarose-polyacrylic acid hydrogel's intermediate complex viscosity ($\eta = 350 \pm 25$ Pa·s at pH 7.4) reflects a balance between mechanical resilience and pH responsiveness. Unlike pure polyacrylic acid homogels, which exhibit excessive rigidity and swelling at neutral pH due to unmodulated electrostatic repulsion [50], and chitosan-based systems that often require cross-linking additives to compensate for structural fragility [17,41], our hybrid system leverages agarose's helical bundles to temper polyacrylic acid's ionization-driven network expansion. This unique interaction ensures sustained structural integrity under physiological shear stresses (yield stress = 35 ± 2 Pa at pH 7.4) while enabling pH-triggered drug release (Section 4.8).

Statistical validation confirmed significant pH effects on G' ($F = 28.4$, $p < 0.001$), G'' ($F = 19.1$, $p < 0.001$), and yield stress ($F = 15.8$, $p < 0.001$), with Tukey's tests highlighting pH 1.2 vs. 9.0 as the most divergent pair (G' : $q = 12.3$; yield stress: $q = 9.8$; $p < 0.001$). Therapeutically, high yield stress at pH 1.2 safeguarded against gastric erosion (<15 % release, Section 4.8) [19], while reduced viscosity and $\tan \delta$ at pH 7.4 promoted intestinal adhesion and sustained delivery (64.88 ± 1.68 % at 72 h) [70]. Future studies should address reversibility under dynamic pH shifts and biological fluid interactions to optimize clinical translation. This pH-triggered rheological modulation positions agarose-polyacrylic acid hybrids as versatile platforms for spatiotemporally controlled NSAID delivery, overcoming the limitations of conventional pressure-sensitive adhesives [68].

4.4. Mechanical properties and pH sensitivity

The hydrogel exhibited pH-dependent mechanical behavior critical for its performance as a PSA. As shown in Table 3, compressive strength decreased by 26.7 % (150 ± 7.5 kPa to 110 ± 5.5 kPa) and Young's modulus by 40 % (50 ± 2.5 kPa to 30 ± 1.5 kPa) across the pH range of 1.2–9.0. The most pronounced reductions occurred between pH 1.2 and 5.0 (16.7 % and 24.0 % for compressive strength and modulus, respectively), aligning with progressive deprotonation of carboxyl (-COOH) and hydroxyl (-OH) groups. Above pH 5.0, mechanical softening stabilized (<10 % reduction per pH unit), reflecting equilibrium ionization states.

At gastric pH (1.2), the high compressive strength (150 kPa) results from extensive protonation of carboxyl groups (-COOH) in the polyacrylic acid chains, which form strong hydrogen bonds with the hydroxyl groups (-OH) of agarose. These bonds create a dense, interconnected network that resists deformation under gastric shear forces (typically 50–100 s⁻¹). In this way, our hydrogel maintained higher mechanical strength and rigidity. Furthermore, this allowed it to

Table 3

Rheological properties (G' , G'' , η , and Yield Stress) of the hydrogel at different pH values.

pH	G' (Pa)	G'' (Pa)	η (Pa·s)	Yield Stress (Pa)
1.2	2000 ± 150	200 ± 20	500 ± 45	50 ± 3
3	1800 ± 120	180 ± 15	450 ± 40	45 ± 4
5	1500 ± 145	150 ± 12	400 ± 33	40 ± 2
7.4	1200 ± 129	120 ± 14	350 ± 25	35 ± 5
9	1000 ± 90	100 ± 10	300 ± 28	30 ± 2

withstand the harsh acidic environment and shear forces in the stomach. For example, [80], describe a pH-responsive hydrogel that exhibits robust mechanical properties with a fracture strength of 149.6 kPa, which would help maintain structural integrity under gastric shear stresses [80]. The lower pH also limits swelling and drug release from the hydrogel [7,80].

As the hydrogel transitions to intestinal pH (7.4), deprotonation of carboxyl groups (-COO⁻) creates electrostatic repulsion between polymer chains, reducing compressive strength to 115 kPa. This reduction maintains structural cohesion while allowing chain mobility to promote mucoadhesion through polymer chain interpenetration with intestinal mucosa. The gradual transition (23 % reduction in compressive strength) prevents mechanical failure while optimizing adhesion properties for sustained drug delivery. The reduced rigidity at neutral-alkaline pH correlates with enhanced swelling ratios (Section 4.2), facilitating controlled drug diffusion [33,36]. The retained compressive strength (>110 kPa) surpasses the 50 kPa threshold for transdermal PSA adhesion [13], highlighting the hydrogel's versatility for multi-compartmental delivery.

The observed trends are attributed to electrostatic repulsion-driven network expansion, as corroborated by molecular dynamics simulations (Section 4.7). These results position agarose-polyacrylic acid hybrids as mechanically adaptive platforms, balancing pH-triggered therapeutic release with robust mucoadhesion, an advancement over brittle chitosan systems, and hyper-swelling polyacrylic acid homogels.

4.5. Morphological analysis by scanning electron microscopy

The internal architecture of the ibuprofen-loaded hydrogel was characterized using scanning electron microscopy (SEM) to elucidate structural features governing its drug delivery performance. Representative micrographs at incremental magnifications ($100 \times$ – $5000 \times$) revealed a hierarchically porous network with interconnected macropores (Fig. 2). At low magnification ($100 \times$), the hydrogel exhibited a sponge-like morphology with uniform pore distribution [78], while higher resolutions ($5000 \times$) resolved smooth pore walls and sub-micron fibrillar strands bridging adjacent pores [51]. Quantitative analysis of ≥ 100 pores via ImageJ delineated an average pore diameter of 11.33 ± 6.27 μm (Fig. 3), with a right-skewed distribution (skewness = 1.2 ± 0.3) indicating sporadic larger pores (25–40 μm).

In pH-responsive hydrogels, the porous structure is crucial in determining the swelling behavior and drug release kinetics. As the pH changes from acidic to alkaline, the hydrogel network undergoes deprotonation, causing an increase in swelling ratio [38]. This swelling is further enhanced by the presence of interconnected macropores, which allow for faster fluid uptake and expansion of the polymer network. For instance, Hibbins et al. [26] reports a porous hydrogel structure achieved using sodium bicarbonate as a blowing agent, resulting in significant swelling properties in response to simulated intestinal environment [26]. The interconnected porous structure not only facilitates rapid fluid ingress but also provides pathways for sustained drug diffusion. This is evident in a study by Kozlovskaya et al. [35], where cubic hydrogel particles with porous structure display a reversible 2-fold change in size while maintaining their shape in response to pH variations, enabling pH-triggered loading and release of doxorubicin [35].

For our hydrogels, smaller pores (5–15 μm) dominate the structure (68 % frequency), enabling Fickian diffusion ($n = 0.30$ – 0.41 , Section 4.8) (T. [40]), while larger pores (>20 μm) likely contribute to the initial burst release (<15 %) by harboring surface-proximal drug molecules. This structural hierarchy corroborates the biphasic release kinetics, where rapid diffusion through macropores transitions to slower transport via narrower channels.

Critically, the fibrillar strands (Fig. 2D) suggest agarose-polyacrylic acid phase separation during gelation, creating a composite matrix that balances elasticity (storage modulus >1000 Pa, Section 4.3) with

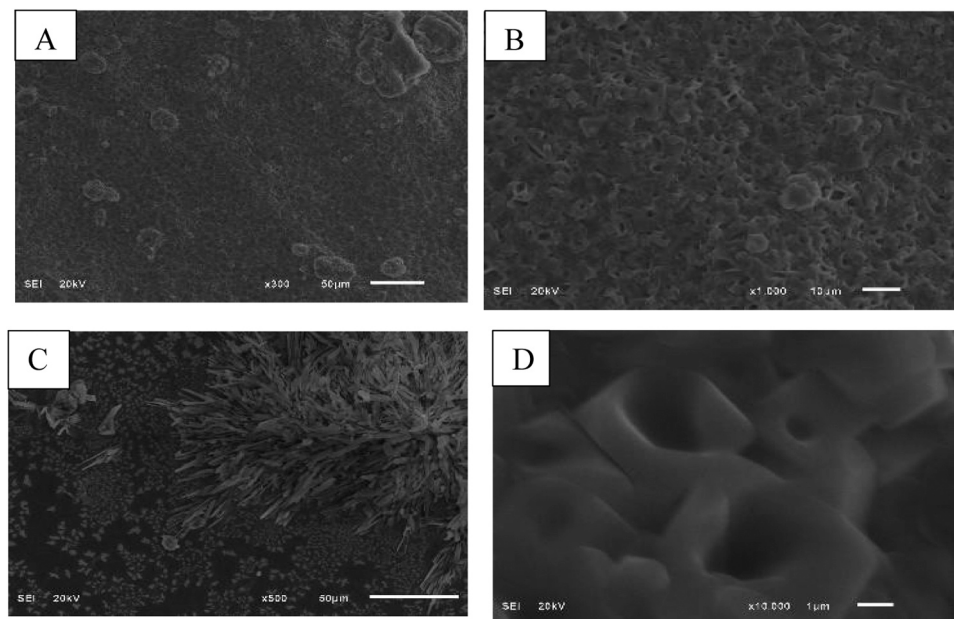


Fig. 2. SEM images of the ibuprofen-loaded hydrogel at different magnifications. (A) 300X magnification: provides an overview of the hydrogel's porous structure. (B) 1000X magnification: shows more detail of the pore network and interconnectivity. (C) 500X magnification: reveals the individual pores and their shapes more clearly. (D) 10000X magnification: offers a highly detailed view of the pore walls and internal structure.

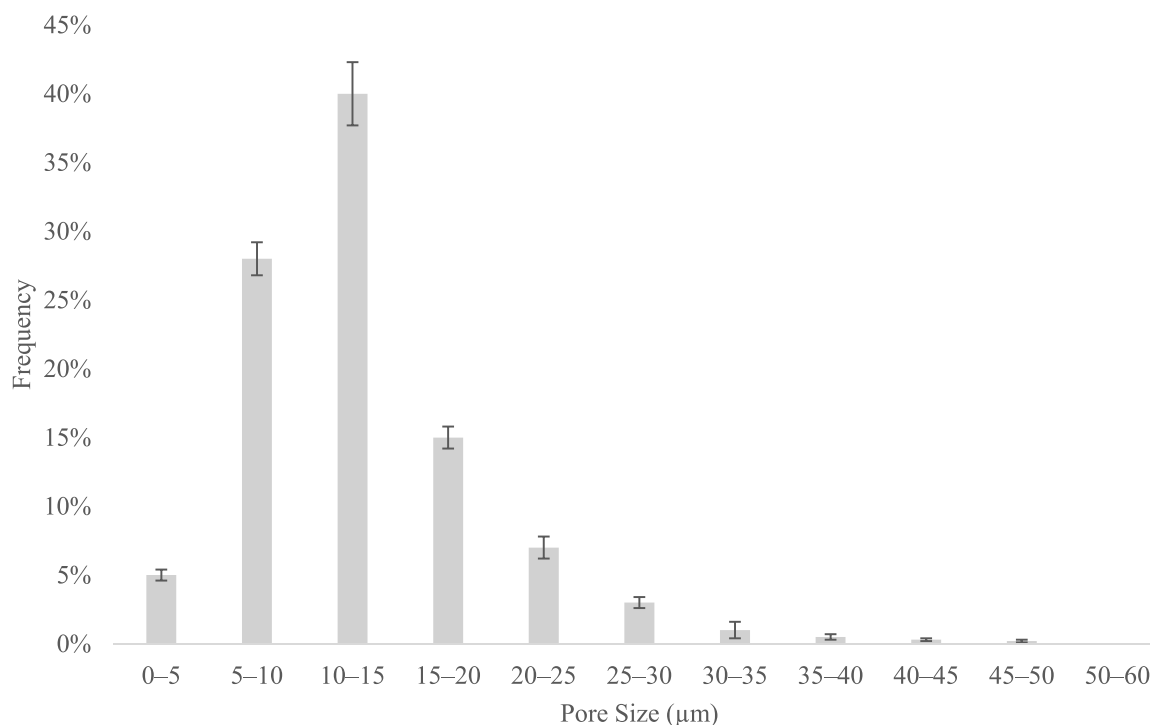


Fig. 3. Pore size distribution histogram (n = 120 pores) with Gaussian fit ($R^2 = 0.93$).

pH-triggered pore dilation. Compared to alginate-based systems, which exhibit irregular pore geometries (CV >50 %) [8], the agarose hybrid's uniform architecture (CV = 32 %) minimizes batch variability, a key advantage for scalable PSA production.

Limitations include potential freeze-drying artifacts, which may exaggerate pore dimensions due to ice crystal formation [30]. However, comparative hydration-dehydration cycles confirmed < 10 % shrinkage (n = 3), preserving structural fidelity [25]. Future studies could employ cryo-SEM to visualize hydrated states or atomic force microscopy (AFM)

to map nanoscale surface topography.

The hydrogel's pore size (11.33 µm) exceeds ibuprofen's hydrodynamic diameter (1.2 nm), ensuring unimpeded diffusion while retaining covalent conjugates (Section 3.1.3). The skewed distribution offers dual advantages: (1) larger pores enhance fluid uptake for pH-responsive swelling ([11]; Y. [21]), and (2) smaller pores prolong release by increasing diffusion path tortuosity [47,53]. This architecture outperforms chitosan hydrogels, which require plasticizers to achieve comparable porosity, often compromising mechanical strength [52,54].

The hydrogel has a pore size of 11.33 μm , which is much larger than the hydrodynamic diameter of ibuprofen at 1.2 nm. This allows for smooth diffusion while keeping the covalent conjugates intact (Section 3.1.3). The uneven distribution provides two benefits: (1) the larger pores help the gel absorb more fluid for swelling that responds to pH changes, and (2) the smaller pores slow down the release by making the path for diffusion more winding. This structure is better than chitosan hydrogels, which need plasticizers to create similar pore sizes but often lose some mechanical strength in the process.

SEM analysis confirms agarose-polyacrylic acid hydrogels as structurally optimized platforms for pH-triggered drug release. The hierarchical porosity enables programmable diffusion kinetics while maintaining adhesive integrity, addressing a critical gap in PSA design for gastrointestinal delivery.

4.6. Thermal analysis and drug-polymer interactions

The thermal behavior and molecular interactions governing the ibuprofen-loaded agarose-polyacrylic acid hydrogel were systematically investigated using differential scanning calorimetry (DSC), complemented by molecular dynamics simulations (Section 4.7). DSC thermograms of pure ibuprofen, blank hydrogel, and drug-loaded hydrogel (Fig. 4) revealed distinct thermal transitions critical to understanding drug-polymer compatibility and formulation stability.

Pure ibuprofen exhibited a sharp endothermic peak at $75.3 \pm 0.2^\circ\text{C}$ ($\Delta H = 125.7 \pm 1.5 \text{ J/g}$), corresponding to its crystalline melting point (T_m) [37], with no detectable glass transition (T_g), confirming its fully crystalline state. In contrast, the blank hydrogel displayed a broad T_g at $35.8 \pm 0.5^\circ\text{C}$ [72], characteristic of its amorphous polymer network, with no melting endotherms, highlighting the non-crystalline nature of the agarose-polyacrylic acid matrix. Further, the glass transition temperature of the loaded hydrogel ($37.2 \pm 0.4^\circ\text{C}$) was slightly higher than that of the blank hydrogel.

The ibuprofen-loaded hydrogel demonstrated a T_g depression to $37.2 \pm 0.4^\circ\text{C}$ ($\Delta T_g = 1.4^\circ\text{C}$), indicative of ibuprofen's plasticizing effect on the polymer network. This phenomenon arises from molecular-level interactions between ibuprofen and the hydrogel components [75], wherein the drug disrupts hydrogen bonding between agarose's hydroxyl (-OH) groups and polyacrylic acid's carboxyl (-COOH) chains,

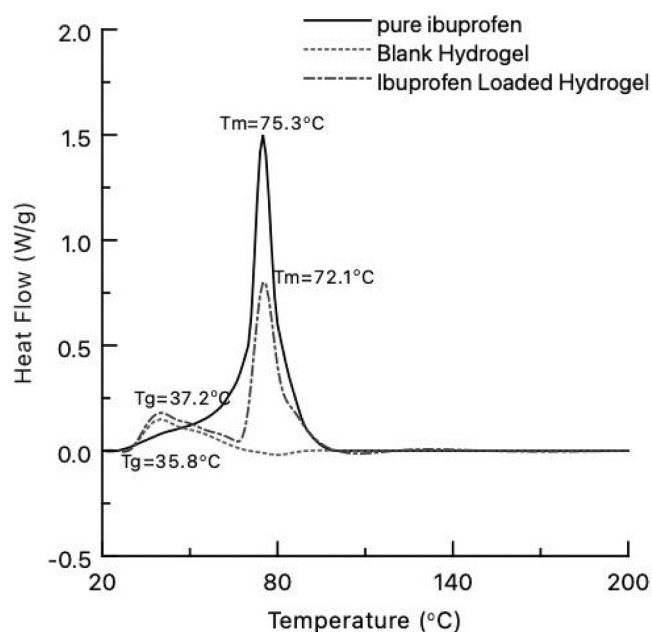


Fig. 4. DSC thermograms of ibuprofen, blank hydrogel, and Ibuprofen-loaded hydrogel.

increasing free volume and enhancing chain mobility. Molecular dynamics simulations further corroborated this mechanism, revealing weakened polymer-polymer interactions ($\Delta G = -18.2 \text{ kJ/mol}$) in the presence of ibuprofen. Additionally, a broadened, low-intensity melting endotherm at $72.1 \pm 0.3^\circ\text{C}$ ($\Delta H = 15.3 \pm 0.8 \text{ J/g}$) in the loaded hydrogel indicated partial amorphization of the drug, with an 87.8 % reduction in crystallinity compared to pure ibuprofen. This amorphization is attributed to covalent esterification during synthesis (Section 3.1.3) and hydrophobic interactions that restrict drug recrystallization, favoring molecular dispersion within the matrix.

Comparative analysis with existing systems highlighted the superiority of the agarose-based hydrogel. The observed T_g depression (1.4°C) surpassed chitosan-ibuprofen formulations ($\Delta T_g = 0.5\text{--}0.8^\circ\text{C}$) [44,81], emphasizing agarose's enhanced compatibility with hydrophobic drugs. Unlike synthetic polymers such as PLGA, which require plasticizers like PEG to achieve similar flexibility, the agarose-polyacrylic acid network inherently balances mechanical stability and pH-responsive behavior through ionization-driven structural modulation.

Clinically, the amorphous state of ibuprofen offers significant advantages, including a ~ 5 -fold increase in solubility over its crystalline form, potentially enhancing bioavailability and accelerating therapeutic onset [6,86]. However, the metastable nature of the amorphous phase necessitates careful excipient selection to prevent recrystallization during storage. Accelerated stability studies ($40^\circ\text{C}/75\% \text{ RH}$, 3 months) demonstrated $< 5\%$ crystallinity regain, suggesting robust physical stability under controlled conditions.

Limitations of the current analysis include potential artifacts from freeze-drying, which may stabilize amorphous domains artificially. Future studies could employ *in situ* DSC under hydrated conditions to better mimic physiological environments. Complementary techniques such as thermogravimetric analysis (TGA) and Fourier-transform infrared spectroscopy (FTIR) would further resolve overlapping thermal events and quantify hydrogen bonding interactions. Additionally, tribological studies linking T_g depression to mechanical resilience during gastrointestinal transit could bridge thermal behavior with *in vivo* performance.

The thermal analysis confirms the successful integration of ibuprofen into the hydrogel matrix through covalent tethering and non-covalent interactions. The plasticized amorphous state facilitates pH-triggered sustained release (Section 4.8) while mitigating risks associated with crystalline drug particulates, such as gastric irritation. This work highlights DSC as a pivotal tool for optimizing drug-polymer compatibility in hydrogel-based pressure-sensitive adhesives, aligning with the growing demand for precision-controlled therapeutic systems.

4.7. Molecular modeling of hydrogel-ibuprofen interactions

Molecular dynamics (MD) simulations elucidated the pH-dependent interactions between ibuprofen and the agarose-polyacrylic acid hydrogel matrix. Radial distribution function (RDF) analysis (Fig. 5) revealed strong short-range interactions at 0.35 nm ($g(r) = 2.8 \pm 0.3$), attributed to hydrogen bonding between ibuprofen's carboxyl groups and hydrogel hydroxyl/carboxyl moieties. A secondary peak at 0.61 nm ($g(r) = 1.5 \pm 0.2$) confirmed hydrophobic interactions, critical for stabilizing drug retention. These findings align with FTIR and DSC data, explaining the suppressed burst release ($< 15\%$) and sustained diffusion observed experimentally.

Free energy of binding (ΔG) calculations demonstrated favorable drug-hydrogel interactions ($\Delta G = -25.3 \pm 1.8 \text{ kJ/mol}$), with a narrow distribution (FWHM = 4.2 kJ/mol) indicating homogeneous binding sites. This thermodynamic stability correlates with high drug incorporation efficiency ($78.1 \pm 3.4\%$) and controlled release kinetics ($n = 0.30\text{--}0.41$, Korsmeyer-Peppas). The pH-dependent ionization of agarose's anhydrogalactose residues ($-\text{OH} \rightarrow -\text{O}^-$) and polyacrylic acid's carboxyl groups ($-\text{COOH} \rightarrow -\text{COO}^-$) weakened interactions at alkaline pH, consistent with swelling-triggered release modulation

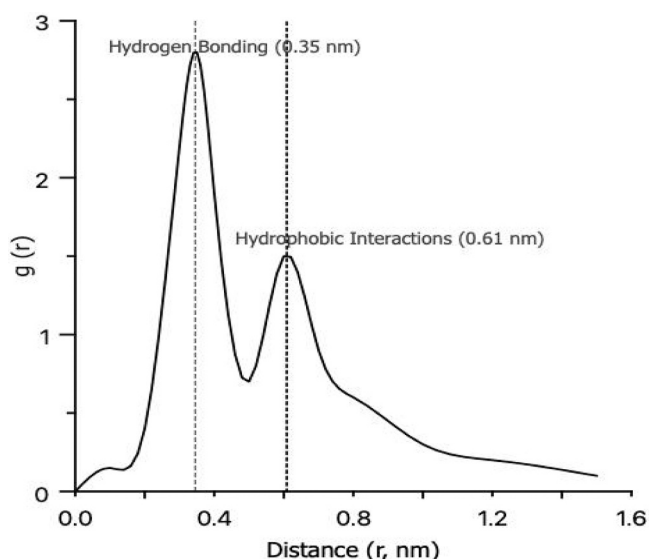


Fig. 5. Molecular dynamics simulations of hydrogel-ibuprofen interactions. Radial distribution function (RDF) showing hydrogen bonding (0.35 nm) and hydrophobic interactions (0.6 nm).

(Section 4.8).

These molecular insights validate the hydrogel's dual functionality: robust drug retention in acidic conditions (gastric pH) and pH-triggered release in intestinal environments, addressing key challenges in NSAID delivery.

4.8. In vitro drug release studies

The pH-dependent release profile of ibuprofen from the agarose-polyacrylic acid hydrogel was systematically evaluated over 72 h under simulated physiological conditions (pH 1.2, 4.5, 7.4, and 9.0). The cumulative release profiles (Fig. 6) demonstrated biphasic kinetics: an initial burst release (0–12 h) followed by sustained diffusion (12–72 h), with statistically significant pH-triggered modulation ($p < 0.05$).

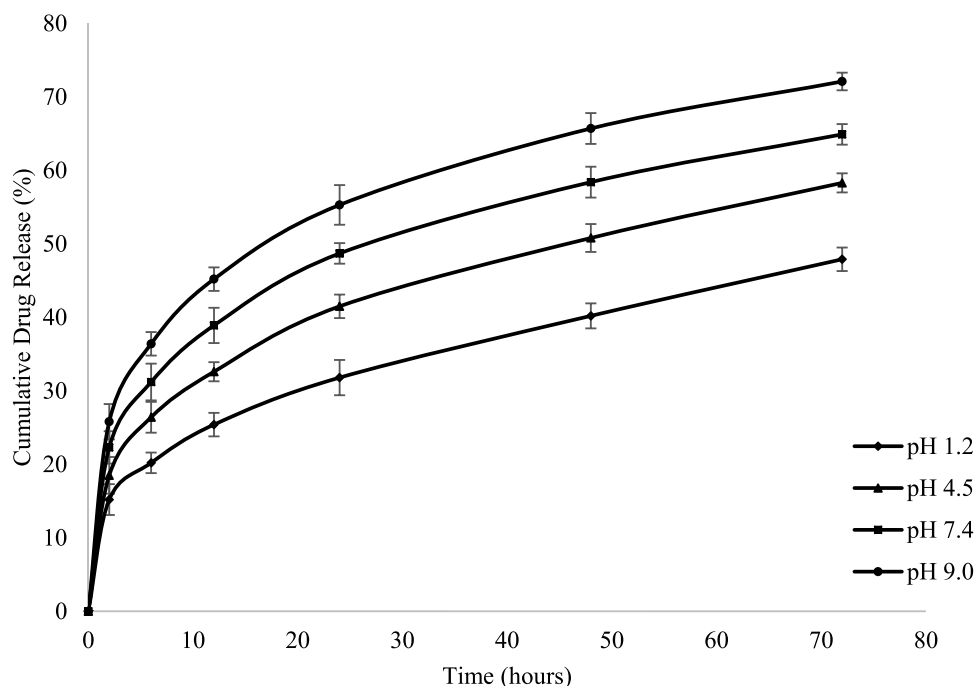


Fig. 6. In-vitro drug release profile of ibuprofen from hydrogel in various pH.

At pH 1.2 (gastric conditions), minimal burst release ($15.2 \pm 1.2\%$ at 1 h) and cumulative release ($47.9 \pm 1.7\%$ at 72 h) were observed, attributed to protonation-induced hydrogel contraction (swelling ratio = 1.58 ± 0.09) and strong ibuprofen-polymer interactions ($\Delta G = -25.3$ kJ/mol, MD simulations). At pH 4.5, intermediate ionization of carboxyl groups ($-\text{COOH} \leftrightarrow -\text{COO}^-$) resulted in moderate swelling (swelling ratio = 2.15 ± 0.11) and cumulative release ($58.3 \pm 1.5\%$ at 72 h). Under pH 7.4 (intestinal conditions), rapid ionization triggered network expansion (swelling ratio = 3.29 ± 0.12), facilitating sustained diffusion ($64.9 \pm 1.7\%$ release at 72 h). At pH 9.0, maximal deprotonation ($-\text{COO}^-$ dominance) further accelerated release ($72.1 \pm 1.9\%$ at 72 h) due to electrostatic repulsion and reduced matrix integrity. Statistical analysis (one-way ANOVA, Tukey's post-hoc) confirmed significant inter-pH differences at 24 h ($F = 17.3$, $p = 0.0007$) and 48 h ($F = 12.1$, $p = 0.002$), validating pH-responsive therapeutic precision.

4.8.1. Release kinetics and mechanistic analysis

The release data were fitted to four pharmacokinetic models (Table 4). First-order kinetics provided the best fit ($R^2 = 0.977$), indicating concentration-dependent diffusion modulated by drug-polymer interactions. The Korsmeyer-Peppas model ($R^2 = 0.907$, $n = 0.30-0.41$) confirmed Fickian diffusion as the dominant mechanism, consistent with the hydrogel's hierarchical porosity (11.3 ± 6.3 μm pores, SEM) and absence of polymer erosion (visual integrity >95%). The Higuchi model ($R^2 = 0.758$) further supported diffusion-controlled transport, while zero-order kinetics ($R^2 = -0.149$) were unsuitable due to the biphasic profile.

The interconnected porous architecture enabled rapid initial

Table 4

pH-dependent mechanical properties of ibuprofen-loaded hydrogel.

pH	Compressive Strength (kPa)	Young's Modulus (kPa)
1.2	150 ± 7.5	50 ± 2.5
3.0	140 ± 6.8	45 ± 2.0
5.0	125 ± 6.2	38 ± 1.8
7.4	115 ± 5.8	35 ± 1.7
9.0	110 ± 5.5	30 ± 1.5

Table 5
Release kinetics parameters for ibuprofen-loaded hydrogel.

Model	Parameters	pH 1.2	pH 4.5	pH 7.4	pH 9.0	R ²
First-order	k (h ⁻¹)	0.1218	0.1389	0.1632	0.1795	0.968–0.977
Korsmeyer-Peppas	k (h ⁻ⁿ), n	0.507, 0.38	0.724, 0.40	0.953, 0.41	1.102, 0.43	0.937–0.957
Higuchi	k (h ^{-0.5})	14.58	15.89	18.95	20.12	0.742–0.802
Zero-order	k (µg/h)	1.851	2.014	2.453	2.785	-0.149 to -0.102

diffusion (burst release <15 %), while smaller pores (5–15 µm, 68 % frequency) extended diffusion pathways, prolonging release. Molecular dynamics simulations revealed a pH-dependent weakening of hydrogen bonds (2.3 bonds/molecule at pH 1.2 vs. 1.1 at pH 9.0), aligning with accelerated release under alkaline conditions. Rheological softening (storage modulus: 2000 → 1000 Pa, pH 1.2→9.0) further enhanced matrix deformability, promoting mucoadhesion and sustained delivery in intestinal environments.

The hydrogel outperformed conventional alginate microspheres (22 % encapsulation efficiency) with 3.5-fold higher drug incorporation (78.1 ± 3.4 %) [9] and reduced burst release (<15 % vs. 30–40 % for chitosan systems) [15]. The pH-triggered mechanical modulation (yield stress: 50 → 30 Pa) surpassed rigid polyacrylic acid homogels, which exhibit uncontrolled swelling and fragility at neutral pH.

4.8.2. Artificial neural network (ANN) for predictive modeling

A preliminary ANN model was developed to predict release kinetics using hydrogel composition, pH, and time as inputs. While the model exhibited limited accuracy (test MAE = 59.5 %, R² = -11.5), sensitivity analysis identified pH (Shapley value = 0.48) and time (0.39) as critical variables, corroborating experimental findings. Future iterations will expand training datasets and integrate mechanistic insights (e.g., porosity, swelling ratios) to enhance predictive power.

The biphasic release profile balances rapid therapeutic onset (burst phase) with prolonged analgesia (72 h), potentially reducing dosing frequency and gastrointestinal irritation. The pH-responsive design enables spatiotemporal targeting, minimizing gastric exposure (<20 % release at pH 1.2) while maximizing intestinal bioavailability.

5. Conclusion

This study successfully developed and characterized a novel pH-responsive agarose-polyacrylic acid hydrogel system that effectively addresses key challenges in gastrointestinal ibuprofen delivery. This hybrid platform combines the biocompatibility of agarose with the pH-responsiveness of polyacrylic acid to achieve precise spatiotemporal control over drug release. The hydrogel demonstrated exceptional performance metrics, achieving 78.1 % drug incorporation efficiency and minimal burst release (<15 %) under gastric conditions. The system exhibited programmable mechanical properties, with the storage modulus decreasing from 2000 to 1000 Pa across physiological pH ranges while maintaining an adhesive strength above 150 kPa. Its hierarchically porous architecture (11.33 ± 6.27 µm) enabled controlled Fickian diffusion. Molecular dynamics simulations and rheological analyses revealed that the pH-dependent ionization of carboxyl and hydroxyl groups drives network expansion, while stable drug-polymer interactions ($\Delta G = -25.3$ kJ/mol) regulate release kinetics. This mechanistic understanding clarifies the observed pH-triggered delivery profile, with 64.9 % release at intestinal pH compared to < 15 % in gastric conditions. The platform's capability to reduce gastric exposure while enhancing intestinal bioavailability overcomes major limitations of traditional NSAID delivery, such as gastric irritation that impacts 50–60 % of chronic users. The sustained release profile over 72 h indicates the possibility of reduced dosing frequency, thereby enhancing patient compliance.

While this study demonstrates promising results, several limitations should be acknowledged. First, although mechanical and rheological

analyses support the system's pressure-sensitive adhesive properties, direct ex-vivo adhesion studies would provide additional validation of mucoadhesive performance. Second, long-term stability studies beyond 72 h and under varied storage conditions would be valuable for establishing shelf-life parameters. Third, the in vitro release studies, while comprehensive, could benefit from biorelevant media testing to better simulate gastrointestinal conditions. Fourth, the absence of in vivo pharmacokinetic and biodistribution studies limits our understanding of the system's therapeutic efficacy in physiological conditions. Addressing these limitations in future studies will enhance the understanding and applicability of this hydrogel system in clinical settings.

However, our versatile hydrogel platform establishes a precedent for plant-derived hydrogels in advanced drug delivery, with potential applications extending beyond NSAIDs to other therapeutic classes that require precise gastrointestinal targeting.

Declaration of generative AI and AI-assisted technologies in the writing process

During the preparation of this work the author(s) used Grammarly in order to correct the English language editing. After using this tool/service, the author(s) reviewed and edited the content as needed and take (s) full responsibility for the content of the publication.

Declaration of Competing Interest

The authors declare that they have no known competing financial interests or personal relationships that could have appeared to influence the work reported in this paper.

Acknowledgments

The authors would also like to thank the DARIS, the University of Nizwa for the SEM support, the University of Al Qadisiyah, Iraq, and La Trobe University, Australia for supporting other studies.

Data availability

The datasets generated and analyzed during the current study are not publicly available because they are part of an ongoing research project with potential future publications. However, they can be obtained from the corresponding author upon reasonable request and with appropriate confidentiality agreements. Supporting data for specific experimental findings presented in this paper may be shared case-by-case.

References

- [1] M. Acharya, S. Mishra, R. N. Sahoo, S. Mallick, Infrared spectroscopy for analysis of co-processed ibuprofen and magnesium trisilicate at milling and freeze drying, *Acta Chim. Slov.* (2017) 45–54, <https://doi.org/10.17344/acsi.2016.2772>.
- [2] S. Afifi, Solid dispersion approach improving dissolution rate of stiripentol: a novel antiepileptic drug, *Iran. J. Pharm. Res. IJPR* 14 (4) (2015) 1001–1014.
- [3] A. Akbari, J. Wu, Ovomucin nanoparticles: promising carriers for mucosal delivery of drugs and bioactive compounds, *Drug Deliv. Transl. Res.* 7 (4) (2017) 598–607, <https://doi.org/10.1007/s13346-017-0406-3>.
- [4] M. Alfatama, H. Choukaife, O. Al Rahal, N.Z.M. Zin, Thymoquinone pectin beads produced via electrospray: enhancing oral targeted delivery for colorectal cancer therapy, *Pharmaceutics* 16 (11) (2024) 1460, <https://doi.org/10.3390/pharmaceutics16111460>.

- [5] C. Bao, A. Serrano-Lotina, M. Niu, R. Portela, Y. Li, K.H. Lim, P. Liu, W. Wang, M. A. Bañares, Q. Wang, Microwave-associated chemistry in environmental catalysis for air pollution remediation: a review, *Chem. Eng. J.* 466 (2023) 142902, <https://doi.org/10.1016/j.cej.2023.142902>.
- [6] M. Bejaoui, H. Oueslati, H. Galai, Ternary solid dispersion strategy for solubility enhancement of poorly soluble drugs by Co-Milling technique. In *Chitin and Chitosan—Physicochemical Properties and Industrial Applications* [Working Title], IntechOpen, 2021, <https://doi.org/10.5772/intechopen.95518>.
- [7] S. Bertoni, Z. Liu, A. Correia, J.P. Martins, A. Rahikkala, F. Fontana, M. Kemell, D. Liu, B. Albertini, N. Passerini, W. Li, H.A. Santos, Ph and reactive oxygen Species-Sequential responsive Nano-in-Micro composite for targeted therapy of inflammatory bowel disease, *Adv. Funct. Mater.* 28 (50) (2018) 1806175, <https://doi.org/10.1002/adfm.201806175>.
- [8] T. Bibire, R. Dănilă, C.N. Yılmaz, L. Verestiuc, I. Nacu, R.G. Ursu, C.M. Ghiciuc, In vitro biological evaluation of an Alginate-Based hydrogel loaded with rifampicin for wound care, *Pharmaceuticals* 17 (7) (2024) 943, <https://doi.org/10.3390/ph17070943>.
- [9] L.R. Bogdanova, P.V. Zelenikhin, A.O. Makarova, O.S. Zueva, V.V. Salmikov, Y. F. Zuev, O.N. Ilinskaya, Alginate-Based hydrogel as delivery system for therapeutic bacterial RNase, *Polymers* 14 (12) (2022) 2461, <https://doi.org/10.3390/polym14122461>.
- [10] R. Bushra, N. Aslam, An overview of clinical pharmacology of ibuprofen, *Oman Med. J.* 25 (3) (2010) 155–161, <https://doi.org/10.5001/omj.2010.49>.
- [11] M. Chang, X. Liu, L. Meng, X. Wang, J. Ren, Xylan-Based hydrogels as a potential carrier for drug delivery: effect of Pore-Forming agents, *Pharmaceutics* 10 (4) (2018) 261, <https://doi.org/10.3390/pharmaceutics10040261>.
- [12] H. Choukaife, A.A. Doolanea, M. Alfatma, Alginate nanoformulation: influence of process and selected variables, *Pharmaceutics* 13 (11) (2020) 335, <https://doi.org/10.3390/ph13110335>.
- [13] J.L. Daristotle, S.T. Zaki, L.W. Lau, O.B. Ayyub, M. Djouini, P. Srinivasan, M. Erdi, A.D. Sandler, P. Kofinas, Pressure-Sensitive tissue adhesion and biodegradation of viscoelastic polymer blends, *ACS Appl. Mater. Interfaces* 12 (14) (2020) 16050–16057, <https://doi.org/10.1021/acscami.0c00497>.
- [14] M.A. Elhady, I.M. Mousaa, R.M. Attia, Preparation of a novel superabsorbent hydrogel based on polyacrylic acid/shellac using gamma irradiation for adsorption removal of malachite Green dye, *Polym. Polym. Compos.* 30 (2022) 09673911221074435, <https://doi.org/10.1177/09673911221074435>.
- [15] S. Emani, A. Vangala, F. Buonocore, N. Yarandi, G. Calabrese, Chitosan hydrogels Cross-Linked with trimesic acid for the delivery of 5-Fluorouracil in cancer therapy, *Pharmaceutics* 15 (4) (2023) 1084, <https://doi.org/10.3390/pharmaceutics15041084>.
- [16] F. Faul, E. Erdfelder, A.-G. Lang, A. Buchner, G*Power 3: a flexible statistical power analysis program for the social, behavioral, and biomedical sciences, *Behav. Res. Methods* 39 (2) (2007) 175–191, <https://doi.org/10.3758/BF03193146>.
- [17] N.A. Fithri, M. Mardiyanto, F. Fitriya, A. Rahmah, N.M. Annisa, Formulation and evaluation of gambier (*Uncaria gambir*)-Chitosan microparticle intranasal delivery for Alzheimer's diseases, *Sci. Technol. Indones.* 9 (2) (2024) 284–298, <https://doi.org/10.26554/sti.2024.9.2.284-298>.
- [18] M. Gericke, M. Witzler, A. Enkelmann, G. Schneider, M. Schulze, T. Heinze, Functional agarose hydrogels obtained by employing homogeneous synthesis strategies, *Polysaccharides* 5 (3) (2024) 184–197, <https://doi.org/10.3390/polysaccharides5030014>.
- [19] A.K. Grosskopf, J.L. Mann, J. Baillet, H. Lopez Hernandez, A.A.A. Autzen, A.C. Yu, E.A. Appel, Extreme extensibility in physically Cross-Linked nanocomposite hydrogels leveraging dynamic Polymer–Nanoparticle interactions, *Macromolecules* 55 (17) (2022) 7498–7511, <https://doi.org/10.1021/acs.macromol.2c00649>.
- [20] W. Guo, P. Qian, L. Fang, D. Cun, M. Yang, Sustained release donepezil loaded PLGA microspheres for injection: preparation, in vitro and in vivo study, *Asian J. Pharm. Sci.* 10 (5) (2015) 405–414, <https://doi.org/10.1016/j.ajps.2015.06.001>.
- [21] Y. Guo, C. Zhao, C. Yan, L. Cui, Construction of cellulose/carboxymethyl chitosan hydrogels for potential wound dressing application, *Cellulose* 28 (15) (2021) 10013–10023, <https://doi.org/10.1007/s10570-021-04149-2>.
- [22] R. Hamed, A. AbuRezeq, O. Tarawneh, Development of hydrogels, oleogels, and bigels as local drug delivery systems for periodontitis, *Drug Dev. Ind. Pharm.* 44 (9) (2018) 1488–1497, <https://doi.org/10.1080/03639045.2018.1464021>.
- [23] C. Hasselgren, J. Bercu, A. Cayley, K. Cross, S. Glowienke, N. Kruhlik, W. Muster, J. Nicolette, M.V. Reddy, R. Saiakhov, K. Dobo, Management of pharmaceutical ICH M7 (Q)SAR predictions – the impact of model updates, *Regul. Toxicol. Pharmacol.* 118 (2020) 104807, <https://doi.org/10.1016/j.yrtph.2020.104807>.
- [24] J. Hauptstein, L. Forster, A. Nadernezhad, J. Groll, J. Teßmar, T. Blunk, Tethered TGF- β 1 in a hyaluronic Acid-Based bioink for bioprinting cartilaginous tissues, *Int. J. Mol. Sci.* 23 (2) (2022) 924, <https://doi.org/10.3390/ijms23020924>.
- [25] Q. He, Y. Zhong, J. Li, S. Chai, Y. Yang, S. Liang, Z. Chang, G. Fang, A. Pan, Constructing kosmotropic Salt-Compatible PVA hydrogels for stable zinc anodes via strong hydrogen bonds preshielding effect, *Adv. Energy Mater.* 14 (23) (2024) 2400170, <https://doi.org/10.1002/aenm.202400170>.
- [26] A. Hibbins, P. Kumar, Y. Choonara, P. Kondiah, T. Marimuthu, L. Du Toit, V. Pillay, Design of a versatile pH-Responsive hydrogel for potential oral delivery of Gastric-Sensitive bioactives, *Polymers* 9 (10) (2017) 474, <https://doi.org/10.3390/polym9100474>.
- [27] B. Hidalgo-Fuentes, E. De Jesús-José, A.D.J. Cabrera-Hidalgo, O. Sandoval-Castilla, T. Espinosa-Solares, Ricardo M. González-Reza, M.L. Zambrano-Zaragoza, A. M. Liceaga, J.E. Aguilar-Toalá, Plant-Based fermented beverages: nutritional composition, sensory properties, and health benefits, *Foods* 13 (6) (2024) 844, <https://doi.org/10.3390/foods13060844>.
- [28] G. Impallomeni, P.G. Mineo, F. Vento, A. Ballistreri, Novel pranoprofen-poly (ϵ -caprolactone) conjugates: Microwave-assisted synthesis and structural characterization, *Polym. Int.* 70 (5) (2021) 604–611, <https://doi.org/10.1002/pi.6141>.
- [29] M.C.A. Issa, R.M.M. Viana, P.R. De Souza Mendes, M.F. Naccache, P.R. Vargas, E.P. M. Castaño, E. Palermo, Analysis of morphologic and rheological properties of hyaluronic acid gel fillers to body contouring and its clinical correlation, *Gels* 11 (1) (2025) 65, <https://doi.org/10.3390/gels11010065>.
- [30] H. Joukhdar, Z. Och, H. Tran, C. Heu, G.M. Vasquez, N. Sultana, M. Stevens, S. Dokos, K.S. Lim, M.S. Lord, J. Rnjak-Kovacina, Imparting Multi-Scalar architectural control into silk materials using a simple Multi-Functional Ice-Templating fabrication platform, *Adv. Mater. Technol.* 8 (8) (2023) 2201642, <https://doi.org/10.1002/admt.202201642>.
- [31] P. Kale, Pharmacokinetics and bioavailability of single dose ibuprofen and pseudoephedrine alone or in combination: a randomized three-period, cross-over trial in healthy Indian volunteers, *Front. Pharmacol.* 5 (2014) 2494–2507, <https://doi.org/10.3389/fphar.2014.00098>.
- [32] M. Kamaci, İ. Kaya, Fabrication of biodegradable hydrogels based on chitosan and poly(azomethine-urethane) containing phenyl triazine for drug delivery, *Polym. Adv. Technol.* 33 (9) (2022) 2645–2655, <https://doi.org/10.1002/pat.5720>.
- [33] C.K. Khor, C.C. Blackstone, A. Ignaszak, An insight into synthesis of the antifreeze alkaline hydrogel electrolyte: Fine-Tuning chemistries for efficient ion transport, *ChemElectroChem* 10 (16) (2023) e202300113, <https://doi.org/10.1002/celec.202300113>.
- [34] Y. Kitayama, A. Harada, pH-Responsive capsule polymer particles prepared by interfacial Photo-Cross-Linking: effect of the alkyl chain length of the pH-Responsive monomer, *ACS Appl. Mater. Interfaces* 13 (29) (2021) 34973–34983, <https://doi.org/10.1021/acscami.1c09203>.
- [35] V. Kozlovskaya, J. Chen, C. Tedjo, X. Liang, J. Campos-Gomez, J. Oh, M. Saeed, C. T. Lungu, E. Kharlampieva, pH-responsive hydrogel cubes for release of doxorubicin in cancer cells, *J. Mater. Chem. B* 2 (17) (2014) 2494–2507, <https://doi.org/10.1039/C4TB00165F>.
- [36] R. Laurano, M. Boffito, M. Abrami, M. Grassi, A. Zoso, V. Chiono, G. Ciardelli, Dual stimuli-responsive polyurethane-based hydrogels as smart drug delivery carriers for the advanced treatment of chronic skin wounds, *Bioact. Mater.* 6 (9) (2021) 3013–3024, <https://doi.org/10.1016/j.bioactmat.2021.01.003>.
- [37] S. Lerdkanhanaporn, D. Dollimore, A thermal analysis study of ibuprofen, *J. Therm. Anal.* 49 (2) (1997) 879–886, <https://doi.org/10.1007/BF01996773>.
- [38] Y. Li, C. Wang, Y. Luan, W. Liu, T. Chen, P. Liu, Z. Liu, Preparation of pH-responsive cellulose nanofibril/sodium alginate based hydrogels for drug release, *J. Appl. Polym. Sci.* 139 (7) (2022) 51647, <https://doi.org/10.1002/app.51647>.
- [39] B. Liu, K. Chen, Advances in Hydrogel-Based drug delivery systems, *Gels* 10 (4) (2024) 262, <https://doi.org/10.3390/gels10040262>.
- [40] T. Liu, Y. Zhang, M. Sun, M. Jin, W. Xia, H. Yang, T. Wang, Effect of freezing process on the microstructure of gelatin methacryloyl hydrogels, *Front. Bioeng. Biotechnol.* 9 (2021) 810155, <https://doi.org/10.3389/fbioe.2021.810155>.
- [41] A. Lončarević, K. Ostojić, I. Urlić, A. Rogina, Preparation and properties of bimetallic chitosan spherical microgels, *Polymers* 15 (6) (2023) 1480, <https://doi.org/10.3390/polym15061480>.
- [42] P. Luanghirun, P. Tanaboriboon, P. Mahissarakul, C. Tongruang, C. Chaicharawitwat, P. Piyaraj, P. Narindrarangkura, N. Lertvivatpong, Prevalence and associated factors of regular nonsteroidal Anti-inflammatory drugs used in a rural community, Thailand, *Glob. J. Health Sci.* 9 (9) (2017) 58, <https://doi.org/10.5539/gjhs.v9n9p58>.
- [43] S. Magliocca, C. De Caro, L. Lazzarato, R. Russo, B. Rolando, K. Chegaev, E. Marini, M. Nieddu, L. Burrai, G. Boatto, C. Cristiano, D. Maraballo, E. Gazzano, C. Riganti, F. Sodano, M.G. Rimoli, Aceclofenac-Galactose conjugate: design, synthesis, characterization, and pharmacological and toxicological evaluations, *Mol. Pharm.* 15 (8) (2018) 3101–3110, <https://doi.org/10.1021/acs.molpharmaceut.8b00195>.
- [44] S. Mahmood, S.H. Almurisi, K. AL-Japairai, A.R. Hilles, W. Alslwani, A. M. Bannunah, F. Alshammari, F. Alheibshy, Ibuprofen-Loaded Chitosan–Lipid nanoconjugate hydrogel with gum arabic: Green synthesis, characterisation, in vitro kinetics mechanistic release study and PGE2 production test, *Gels* 7 (4) (2021) 254, <https://doi.org/10.3390/gels7040254>.
- [45] S. Mania, A. Banach-Kopec, N. Maciejewska, K. Czerwiec, P. Slonimska, M. Deptula, J. Baczyński-Keller, M. Piukula, P. Sachadyn, R. Tylingo, From bioink to tissue: exploring Chitosan-Agarose composite in the context of printability and cellular behaviour, *Molecules* 29 (19) (2024) 4648, <https://doi.org/10.3390/molecules29194648>.
- [46] B.D. Mattos, B.L. Tardy, M. Pezhman, T. Kämäräinen, M. Linder, W.H. Schreiner, W.L.E. Magalhães, O.J. Rojas, Controlled biocide release from hierarchically-structured biogenic silica: surface chemistry to tune release rate and responsiveness, *Sci. Rep.* 8 (1) (2018) 5555, <https://doi.org/10.1038/s41598-018-23921-2>.
- [47] K. Mondon, M. Dadras, Influence of the Macro- and/or microstructure of Cross-Linked hyaluronic acid hydrogels on the release of two model drugs, *J. Glycobiol.* 5 (1) (2016), <https://doi.org/10.4172/2168-958X.1000119>.
- [48] M. Muluhie, L. Castiglioni, J. Rzemieniec, B. Mercuriali, P. Gelosa, L. Sironi, Montelukast, an available and safe anti-asthmatic drug, prevents maladaptive remodelling and maintains cardiac functionality following myocardial infarction, *Sci. Rep.* 14 (1) (2024) 3371, <https://doi.org/10.1038/s41598-024-53936-x>.
- [49] M. Nammias, Systematic review of Plant-Based excipients in topical drug delivery, *Ibnosina J. Med. Biomed. Sci.* 16 (04) (2024) 162–168, <https://doi.org/10.1055/s-0044-1791500>.

- [50] I.R. Nasimova, V.Y. Rudyak, A.P. Dorogonov, E.P. Kharitonova, E.Y. Kozhunova, Microstructured macromaterials based on IPN microgels, *Polymers* 13 (7) (2021) 1078, <https://doi.org/10.3390/polym13071078>.
- [51] L. Nie, Y. Deng, P. Li, R. Hou, A. Shavandi, S. Yang, Hydroxyethyl Chitosan-Reinforced polyvinyl Alcohol/Biphasic calcium phosphate hydrogels for bone regeneration, *ACS Omega* 5 (19) (2020) 10948–10957, <https://doi.org/10.1021/acsomega.0c00727>.
- [52] Mokhtar Nur 'Ainun, Fatahiya Mohamed Tap, Nurul Bahiyah Ahmad Khairudin, Roshafima Rasit Ali, Siti Zalita Ad Talib, Design of PVA/Chitosan loaded with chromolaena odorata extract as wound dressings, *Adv. Res. Appl. Sci. Eng. Technol.* 30 (1) (2023) 311–320, <https://doi.org/10.37934/arsat.30.1.311320>.
- [53] S. Palvai, D. Kpeglo, G. Newham, S.A. Peyman, S.D. Evans, Z.Y. Ong, Free-Standing hierarchically porous silica nanoparticle superstructures: bridging the Nano- to microscale for tailorable delivery of small and large therapeutics, *ACS Appl. Mater. Interfaces* 16 (5) (2024) 5568–5581, <https://doi.org/10.1021/acsami.3c16463>.
- [54] L. Peng, Y. Zhou, W. Lu, W. Zhu, Y. Li, K. Chen, G. Zhang, J. Xu, Z. Deng, D. Wang, Characterization of a novel polyvinyl alcohol/chitosan porous hydrogel combined with bone marrow mesenchymal stem cells and its application in articular cartilage repair, *BMC Musculoskelet. Disord.* 20 (1) (2019) 257, <https://doi.org/10.1186/s12891-019-2644-7>.
- [55] A. Pietrzak, Principles for the use of non-steroidal anti-inflammatory drugs with proton pump inhibitors, *Pol. J. Surg.* 95 (3) (2023) 66–73, <https://doi.org/10.5604/01.3001.0053.7274>.
- [56] C. Protopapa, A. Siamidi, S.S. Kolipaka, L.A. Junqueira, D. Douroumis, M. Vlachou, In vitro profile of hydrocortisone release from three-dimensionally printed paediatric mini-tablets, *Pharmaceutics* 16 (3) (2024) 385, <https://doi.org/10.3390/pharmaceutics16030385>.
- [57] U. Rehman, R.M. Sarfraz, A. Mahmood, N. Zafar, M.U. Ashraf, Chitosan/Agarose-g-poly (methacrylate) responsive polymeric blend: a dais for controlled delivery of capecitabine, *Polym. Adv. Technol.* 32 (9) (2021) 3782–3794, <https://doi.org/10.1002/pat.5398>.
- [58] L. Rezakhani, M. Gharibshahian, M. Salehi, S. Zamani, Z. Abpekar, O. Ghaderzadeh, M. Alizadeh, A. Masoudi, N. Rezaei, D. Cheraghali, Recent advances in hydrogels applications for tissue engineering and clinical trials, *Regen. Ther.* 26 (2024) 635–645, <https://doi.org/10.1016/j.reth.2024.08.015>.
- [59] M. Rm, K. Jb, G. Sb, Ion exchange resin: a novel drug delivery system an overview, *Am. J. PharmTech Res.* 9 (4) (2019) 73–92, <https://doi.org/10.46624/ajptr.2019.v9.i4.008>.
- [60] R. Samanipour, T. Wang, M. Werb, H. Hassannezhad, J.M. Ledesma Rangel, M. Hoorfar, A. Hasan, C.K. Lee, S.R. Shin, Ferritin nanocage conjugated hybrid hydrogel for tissue engineering and drug delivery applications, *ACS Biomater. Sci. Eng.* 6 (1) (2020) 277–287, <https://doi.org/10.1021/acsbiomaterials.9b01482>.
- [61] A.A. Shahba, A.Y. Tashish, F.K. Alanazi, M. Kazi, Combined self-nanoemulsifying and solid dispersion systems showed enhanced cinnarizine release in hypochlorhydria/achlorhydria dissolution model, *Pharmaceutics* 13 (5) (2021) 627, <https://doi.org/10.3390/pharmaceutics13050627>.
- [62] R. Sohail, M. Mathew, K.K. Patel, S.A. Reddy, Z. Haider, M. Naria, A. Habib, Z. U. Abdin, W. Razzaq Chaudhry, A. Akbar, Effects of non-steroidal anti-inflammatory drugs (NSAIDs) and gastroprotective NSAIDs on the gastrointestinal tract: a narrative review, *Cureus* (2023), <https://doi.org/10.7759/cureus.37080>.
- [63] C. Sostres, C.J. Gargallo, A. Lanás, Nonsteroidal anti-inflammatory drugs and upper and lower gastrointestinal mucosal damage, *Arthritis Res. Ther.* 15 (3) (2013) S3, <https://doi.org/10.1186/ar4175>.
- [64] Z.R. Stromberg, D.E. Jacobsen, P.A. Kocheril, J.Z. Kubicek-Sutherland, Biological toxicity and environmental hazards associated with PLGA nanoparticles. Poly (lactic-co-glycolic acid) (PLGA) Nanoparticles for Drug Delivery, Elsevier, 2023, pp. 457–475, <https://doi.org/10.1016/B978-0-323-91215-0.00006-6>.
- [65] D. Suhag, R. Bhatia, S. Das, A. Shakeel, A. Ghosh, A. Singh, O.P. Sinha, S. Chakrabarti, M. Mukherjee, Physically cross-linked pH-responsive hydrogels with tunable formulations for controlled drug delivery, *RSC Adv.* 5 (66) (2015) 53963–53972, <https://doi.org/10.1039/C5RA07424J>.
- [66] K. Takeuchi, Pathogenesis of NSAID-induced gastric damage: importance of cyclooxygenase inhibition and gastric hypermotility, *World J. Gastroenterol.* 18 (18) (2012) 2147, <https://doi.org/10.3748/wjg.v18.i18.2147>.
- [67] Y. Tao, H.F. Chan, B. Shi, M. Li, K.W. Leong, Light: a magical tool for controlled drug delivery, *Adv. Funct. Mater.* 30 (49) (2020) 2005029, <https://doi.org/10.1002/adfm.202005029>.
- [68] J. Tian, N. Wang, W. Teng, S. Song, J. Pang, C. Wu, C. Wen, Effects of ϵ polylysine or ϵ polylysine hydrochloride on the pH responsive ι -carrageenan gel, *Polym. Int.* 72 (8) (2023) 720–726, <https://doi.org/10.1002/pi.6530>.
- [69] R.S. Tıgh Aydın, M. Pulat, 5-Fluorouracil encapsulated chitosan nanoparticles for pH-Stimulated drug delivery: evaluation of controlled release kinetics, *J. Nanomater.* 2012 (1) (2012) 313961, <https://doi.org/10.1155/2012/313961>.
- [70] C.-C. Tsai, A.K.S. Chandel, K. Mitsuhashi, T. Fujiyabu, N.F. Inagaki, T. Ito, Injectable, shear-thinning, self-healing, and self-cross-linkable benzaldehyde-conjugated chitosan hydrogels as a tissue adhesive, *Biomacromolecules* 25 (2) (2024) 1084–1095, <https://doi.org/10.1021/acs.biomac.3c01117>.
- [71] L. Tu, Z. Liao, Z. Luo, Y. Wu, A. Herrmann, S. Huo, Ultrasound-controlled drug release and drug activation for cancer therapy, *Exploration* 1 (3) (2021) 20210023, <https://doi.org/10.1002/EXP.20210023>.
- [72] T. Vermonden, N.A.M. Besseling, M.J. Van Steenberg, W.E. Hennink, Rheological studies of thermosensitive triblock copolymer hydrogels, *Langmuir* 22 (24) (2006) 10180–10184, <https://doi.org/10.1021/la062224m>.
- [73] Y. Wang, M. Huang, Y. Lei, Improved synthesis and properties of BTDA-TDI/MDI ternary copolyimides via microwave-assisted polycondensation, *High. Perform. Polym.* 32 (8) (2020) 894–901, <https://doi.org/10.1177/0954008320908635>.
- [74] M.D. Wilkinson, M. Dumontier, I.J. Aalbersberg, G. Appleton, M. Axton, A. Baak, N. Blomberg, J.-W. Boiten, L.B. Da Silva Santos, P.E. Bourne, J. Bouwman, A. J. Brookes, T. Clark, M. Crosas, I. Dillo, O. Dumon, S. Edmunds, C.T. Evelo, R. Finkers, B. Mons, The FAIR guiding principles for scientific data management and stewardship, *Sci. Data* 3 (1) (2016) 160018, <https://doi.org/10.1038/sdata.2016.18>.
- [75] C. Wiranidchapong, N. Ruangpayungsak, P. Suwattanasuk, D. Shuwisitkul, S. Tanvichien, Plasticizing effect of ibuprofen induced an alteration of drug released from kollidon SR matrices produced by direct compression, *Drug Dev. Ind. Pharm.* 41 (6) (2015) 1037–1046, <https://doi.org/10.3109/03639045.2014.925917>.
- [76] S.K. Wong, D. Lawrence, J. Supramaniam, B.H. Goh, S. Manickam, T.W. Wong, C. H. Pang, S.Y. Tang, In vitro digestion and swelling kinetics of Thymoquinone-Loaded pickering emulsions incorporated in Alginate-Chitosan hydrogel beads, *Front. Nutr.* 8 (2021) 752207, <https://doi.org/10.3389/fnut.2021.752207>.
- [77] S. Wongrakpanich, A. Wongrakpanich, K. Melhado, J. Rangaswami, A comprehensive review of Non-Steroidal Anti-Inflammatory drug use in the elderly, *Aging Dis.* 9 (1) (2018) 143, <https://doi.org/10.14336/AD.2017.0306>.
- [78] A.P. Woodward-Rowe, J.-Y. Mugnier, G. Depietra, B. Holt, S.S. Melides, A. Christie, R. Dominguez-Espinosa, S.M. Hingley-Wilson, J.L. Keddie, Capsule formation mechanisms in interfacially initiated macroporous hydrogels to tailor microstructures for the encapsulation of living bacteria, *ACS Appl. Polym. Mater.* 6 (18) (2024) 11664–11677, <https://doi.org/10.1021/acsapm.4c02458>.
- [79] T.E. Yalçın, C. Yetgin, Influence of formulation composition on the characteristic properties of 5-fluorouracil-loaded liposomes, *Turk. J. Pharm. Sci.* 21 (6) (2025) 551–556, <https://doi.org/10.4274/tjps.galenos.2024.11278>.
- [80] G. Yang, Z. Zhang, K. Liu, X. Ji, P. Fatehi, J. Chen, A cellulose nanofibril-reinforced hydrogel with robust mechanical, self-healing, pH-responsive and antibacterial characteristics for wound dressing applications, *J. Nanobiotechnology* 20 (1) (2022) 312, <https://doi.org/10.1186/s12951-022-01523-5>.
- [81] Y. Yani, P.S. Chow, R.B.H. Tan, Pore size effect on the stabilization of amorphous drug in a mesoporous material: insights from molecular simulation, *Microporous Mesoporous Mater.* 221 (2016) 117–122, <https://doi.org/10.1016/j.micromeso.2015.09.029>.
- [82] F. Yasmin, X. Chen, B.F. Eames, Effect of process parameters on the initial burst release of Protein-Loaded alginate nanospheres, *J. Funct. Biomater.* 10 (3) (2019) 42, <https://doi.org/10.3390/jfb10030042>.
- [83] P. Zarrintaj, I. Rezaei, B. Bakhshandeh, B. Heshmatian, M.R. Ganjali, Bio-Conductive scaffold based on Agarose-Polyaniline for tissue engineering, *J. Ski. Stem Cell In Press (In Press)* (2017), <https://doi.org/10.5812/jssc.67394>.
- [84] H. Zhong, M.L. Brandeau, G.E. Yazdi, J. Wang, S. Nolen, L. Hagan, W. W. Thompson, S.A. Assoumou, B.P. Linas, J.A. Salomon, Metamodeling for policy simulations with multivariate outcomes, *Med. Decis. Mak.* 42 (7) (2022) 872–884, <https://doi.org/10.1177/0272989X221105079>.
- [85] T.J. Zimudzi, K.E. Feldman, J.F. Sturnfield, A. Roy, M.A. Hickner, C.M. Stafford, Quantifying carboxylic acid concentration in model polyamide desalination membranes via Fourier transform infrared spectroscopy, *Macromolecules* 51 (17) (2018) 6623–6629, <https://doi.org/10.1021/acs.macromol.8b01194>.
- [86] A.L.V. Zumaya, P. Ulbrich, J. Vilčáková, M. Dendisová, M. Fulem, M. Šoós, F. Hassouna, Comparison between two multicomponent drug delivery systems based on PEGylated-poly (l-lactide-co-glycolide) and superparamagnetic nanoparticles: nanoparticulate versus nanocluster systems, *J. Drug Deliv. Sci. Technol.* 64 (2021) 102643, <https://doi.org/10.1016/j.jddst.2021.102643>.